NOAA Technical Memorandum OAR/ATDD-234

Evaluation of the REEDM Climatological Turbulence Algorithm Using Aircraft Measurements

Richard M. Eckman

Air Resources Laboratory
Silver Spring, Maryland
March 2000

Evaluation of the REEDM Climatological Turbulence Algorithm Using Aircraft Measurements

Richard M. Eckman
Atmospheric Turbulence and Diffusion Division
Oak Ridge, Tennessee

Air Resources Laboratory
Silver Spring, Maryland
March 2000

NOTICE

Mention of a commercial company or product does not constitute an endorsement by NOAA/ERL. Use for publicity or advertising purposes, of information from this publication concerning proprietary products or the tests of such products, is not authorized.

Contents

(blank page)

Evaluation of the REEDM Climatological Turbulence Algorithm Using Aircraft Measurements

Richard M. Eckman

ABSTRACT. During three experiment sessions conducted at Cape Canaveral, Florida in 1995 and 1996, an instrumented light aircraft was used to collect turbulence measurements at various altitudes within and above the boundary layer. In this report, the airborne turbulence measurements are used to evaluate the climatological turbulence algorithm built into the REEDM dispersion model. REEDM is used operationally at the Cape to estimate rocket exhaust cloud dispersion.

Over the ocean and inland waterways near the Cape, the REEDM algorithm frequently overestimated the turbulence levels by a factor of two or more. The algorithm's performance over land surfaces was somewhat better, but even there the performance varied widely as a function of stability. Tests were also performed to determine whether better turbulence estimates could be obtained at the Cape with on-site turbulence measurements. These tests involved the vertical extrapolation of near-surface sonic anemometer turbulence measurements. The on-site measurements were a significant improvement over the REEDM algorithm for boundary-layer turbulence over the ocean and inland waterways. Over land, the on-site measurements led to improved estimates of the horizontal turbulence fluctuations, but not the vertical fluctuations. The findings in this report support the contention that improved operational turbulence estimates could be obtained at the Cape by installing on-site turbulence instrumentation.

1. Introduction

The U. S. Air Force has rocket launch facilities both on the East Coast of the U. S. at Cape Canaveral Air Station, Florida and on the West Coast at Vandenberg Air Force Base, California. Both facilities have nearby populated areas that can potentially be affected by the exhaust clouds emitted during rocket launches. To minimize the risks and environmental impacts associated with the launch clouds, the Air Force uses a dispersion model called REEDM (Rocket Exhaust Effluent Diffusion Model, see Bjorklund 1990) to estimate the effluent transport and diffusion. REEDM was first released in the early 1980s, but it has roots extending back to earlier modeling efforts in the late 1960s and 1970s. It divides the dispersion of the rocket exhaust into two phases: a buoyant-rise phase and a passive-diffusion phase. The buoyant-rise phase represents the initial ascent of the cloud as

a result of its high temperature. The passive-diffusion phase represents the later transport and diffusion resulting from the ambient atmospheric winds and turbulence.

In the passive-diffusion phase, REEDM requires an estimate of the turbulence levels at the altitudes where the cloud is located. The main turbulence parameters of interest are the standard deviations σ_A and σ_E of the wind direction in respectively the horizontal and vertical directions. These parameters can be estimated either with direct on-site measurements or with a climatological algorithm that is built into REEDM (Bjorklund 1990). Currently, on-site turbulence measurements are being employed at the Vandenberg facility, but the built-in algorithm is still used at Cape Canaveral.

Although REEDM has been used operationally for many years, there was some concern within the Air Force that it had not been externally peer reviewed and had not been evaluated using data collected at the launch facilities. The Model Validation Program (MVP, Start and Hoover 1995; Kamada et al. 1997) was created to address these concerns. An early stage of MVP was an external verification and sensitivity study of REEDM (Eckman et al. 1996). Between 1995 and 1997, MVP conducted a series of four field-experiment sessions at the launch facilities. Three were at Cape Canaveral (1995–1996) and one was at Vandenberg (1997). These sessions included surface- and aircraft-based meteorological measurements and the release of SF_6 tracer from fixed surface locations and from a blimp circling at fixed altitudes.

One of the instrument platforms that contributed to all four MVP field sessions was a light aircraft operated by the Atmospheric Turbulence and Diffusion Division of NOAA's Air Resources Laboratory (Crawford and Dobosy 1992; Eckman et al. 1999). This aircraft, a homebuilt design called a Long-EZ, can measure a wide variety of atmospheric variables, including the mean winds and turbulence parameters. The ability of the NOAA Long-EZ to measure turbulence levels at various altitudes provides an excellent opportunity to evaluate the performance of the REEDM turbulence algorithm at the launch facilities.

In this report, measurements of σ_A and σ_E taken with the Long-EZ at Cape Canaveral are used to evaluate the climatological turbulence algorithm that is built into REEDM. Two different comparisons are performed using different sources of input to the REEDM algorithm. First, the algorithm is run using mean-wind profiles from the Long-EZ as input; this is considered a "best case" scenario, because the mean-wind profiles are co-located with the turbulence measurements both in space and time. Second, the REEDM algorithm is evaluated using rawinsonde wind profiles as input. Since the rawinsonde profiles are not co-located with the aircraft measurements in space and (usually) time, it is expected that the algorithm's performance should be degraded relative to the "best-case" scenario.

Climatological turbulence algorithms such as the one built into REEDM are still commonly used, but the meteorological community has increasingly favored the use of on-site turbulence measurements (Hanna et al. 1977, 1982; Irwin 1983). On-site measurements were also recommended at the Cape by Eckman et al. (1996). However, there is no guarantee that on-site measurements will improve the performance of a dispersion model.

Poor instrument placement, for example, can hamper the utility of turbulence measurements, as can improper processing of the measurements. (*e.g.*, the range of turbulence eddy sizes that is resolved by the measurements must be consistent with the dispersion model's assumptions.)

The utility of on-site turbulence measurements at the Cape is put to the test in this report by comparing the σ_A and σ_E estimates produced by the REEDM algorithm with those obtained by extrapolating surface turbulence measurements upward through the depth of the boundary layer. During the MVP sessions at the Cape, sonic anemometers were placed on towers at several different locations. Turbulence measurements from these instruments are extrapolated upward using well-known formulas from the open literature and then compared with the Long-EZ measurements. The intent of this comparison is to determine whether dispersion estimates can be improved by adding routine surface-based turbulence measurements at the Cape.

In addition to evaluating turbulence estimates, the report also investigates the spatial variability of the turbulence at the Cape. This is an important issue, since REEDM assumes that the turbulence does not vary horizontally.

2. Long-EZ Measurements

Only a brief description of the NOAA Long-EZ aircraft is given here, since the aircraft itself and the operating principals of its major sensors have been documented elsewhere (Brown et al. 1983; Auble and Meyers 1992; Crawford and Dobosy 1992; Eckman et al. 1999). The aircraft is designed to carry two passengers and uses a pusher engine configuration. It has a gross weight of 725 kg. During data collection, the aircraft typically flies at air speeds of 50–60 $\mathrm{m\,s^{-1}}$.

The Long-EZ took part in all three MVP sessions at Cape Canaveral. Sessions 1 and 2 occurred respectively in July and October 1995, whereas Session 3 took place in April–May 1996. A series of instrument failures limited the amount of usable turbulence data from Session 1. Sessions 2 and 3 were significantly more successful.

As shown in Fig. 1, the earth's surface near Cape Canaveral is a patchwork of land, sea, lakes, and other wetlands. This surface heterogeneity can lead to rather complex wind patterns at the Cape, including sea breezes (Reed 1979; Atkins et al. 1995; Atkins and Wakimoto 1997) and converging winds that can initiate thunderstorm development (Byers and Rodebush 1948; Neumann 1971). To account for this heterogeneity, the Long-EZ often flew a series of straight flight legs over specific surface types. Figure 2, for example, shows three flight legs commonly flown during MVP Session 3. The T–J leg represents a land surface, E–D represents the sea, and N–S–U represents the shallow inland waterways near the Cape. A similar set of legs was flown in Session 2, although the E–D leg was further out to sea. These legs were flown at various altitudes from about 30 m to 1700 m AGL.

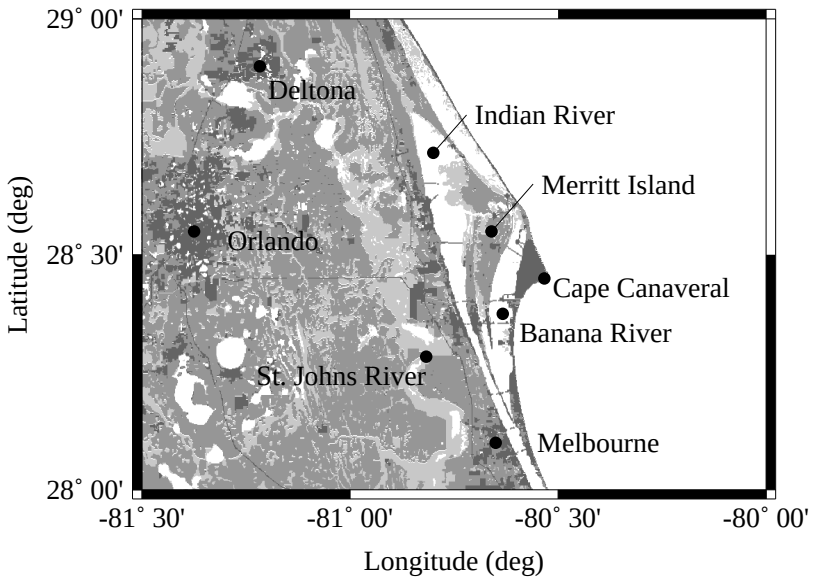

Figure 1: Land-use map of eastern central Florida. The various shades represent water (white), wetlands (lightest grey), forest and fields (intermediate grey), and urban/industrial areas (darkest grey).

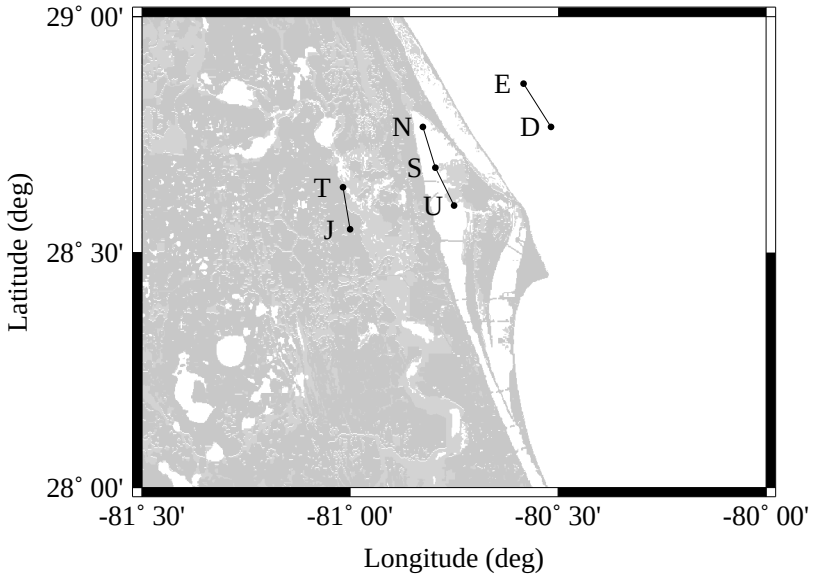

Figure 2: Aircraft flight legs used during MVP Session 3.

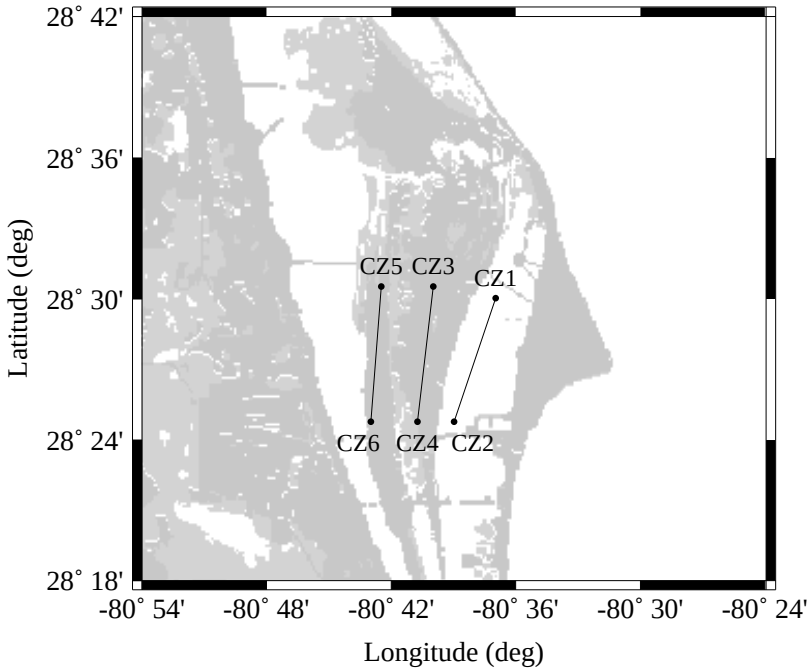

Figure 3: Waypoints used to investigate the Merritt Island convergence zone during MVP Session 3.

During some Session 3 flights, the Long-EZ flew the "convergence-zone" flight legs shown in Fig. 3. These were intended to investigate the presence of a convergence zone over Merritt Island.

For the REEDM evaluations in this report, all the available Long-EZ data that were available from flight legs resembling those in Figs. 2 and 3 were used. Given the hardware problems and the different type of flight legs used in Session 1 (Eckman et al. 1999), no data from this session are included. The remaining data from the other sessions can be divided into five groups according to the prevailing surface type and proximity to the coast: inland data from the T–J leg, sea data from the E–D and similar legs, data from the Indian River N–S–U leg, data from the Banana River CZ1–CZ2 leg, and data from the Merritt Island CZ3-CZ4 and CZ5-CZ6 legs. This grouping into inland, sea, Indian River, Banana River, and Merritt Island data sets will be used throughout this report.

Both the inland and Merritt Island data were collected over a land surface. However, Merritt Island is closer to the coast and surrounded by waterways, so the turbulence there may be different from that observed inland. Likewise, the Indian River and Banana River turbulence may differ even though both locations are over waterways.

In all, 781 individual passes along the various flight legs are available for evaluating the REEDM turbulence estimates. These passes represent a variety of atmospheric conditions,

including both convective and stable boundary layers. Most of the MVP data were collected during the day, so there are more data available for unstable and near-neutral atmospheric conditions than for stable conditions. The data also cover altitudes both within and above the boundary layer.

To compute estimates of σ_A and σ_E from the Long-EZ data, a program called `makestats` (Eckman et al. 1999) was used. Among other variables, this program uses the Long-EZ velocity time series to compute the mean wind speed $\overline{U}$, the standard deviation σ_v of the horizontal velocity component that is perpendicular to the mean wind direction, and the standard deviation σ_w of the vertical velocity component. The directional standard deviations are then computed as

$$\sigma_A = \frac{\sigma_v}{\overline{U}} ; \tag{1}$$

$$\sigma_E = \frac{\sigma_w}{\overline{U}} . \tag{2}$$

The program allows the user to specify the sampling time Λ used in computing the turbulence statistics. This sampling time affects the range of turbulence eddy sizes that is included in the fluctuation statistics.

In computing σ_A and σ_E, a question arises concerning the appropriate Λ for ensuring that the observations and the REEDM estimates are not mismatched. According to the REEDM User's Manual (Bjorklund 1990), the default sampling time for the REEDM estimates is 600 s. Eckman (1994a) pointed out, however, that it is physically more accurate to consider a sampling distance D rather than a sampling time Λ. For measurements at fixed towers, the sampling distance is $D = \overline{U}\Lambda$. Two separate turbulence measurements can be considered to be matched regarding their sampling characteristics if they have the same values of D. This means, for example, that even if two tower measurements have the same values of Λ, their sampling characteristics are still dissimilar unless they also have the same mean wind speed $\overline{U}$.

In spite of the problems with using a sampling time Λ rather than a distance D, the fact remains that REEDM uses the default $\Lambda = 600$ s. This means D varies with the wind speed. The Long-EZ measurements can still be compared with the REEDM estimates as long as it is ensured that the measurements and model estimates both use the same value of D. For aircraft measurements, the sampling distance is the product of the aircraft's true air speed V_a and the sampling time Λ_a. Thus, the aircraft measurements and REEDM estimates will have equivalent values of D if

$$V_a \Lambda_a = \overline{U} \Lambda_R , \tag{3}$$

where $\Lambda_R = 600$ s is the sampling time assumed in REEDM. Since V_a, $\overline{U}$, and Λ_R are all known for each pass along a flight leg, the appropriate value of Λ_a can be computed.

Table 1: Net radiation index as a function of solar altitude a.

Range of solar altitude a	Net Radiation Index
$a > 60°$	4
$35° < a \leq 60°$	3
$15° < a \leq 35°$	2
$0° < a \leq 15°$	1

3. REEDM Turbulence Algorithm

REEDM uses a turbulence algorithm based on net-radiation and wind-speed classifications similar to those developed by Turner (1964). The basic input variables are the solar elevation, cloud cover, cloud ceiling, and the near-surface wind speed. The first three of these are used to compute a net radiation index (NRI) as described below.

1. If the cloud cover is 10/10 and the cloud ceiling is less than 2134 m, the NRI is zero for both day and night.
2. For nighttime when the cloud cover is less than 10/10 or the ceiling is greater than 2134 m, the NRI is -1.
3. For daytime when the cloud cover is $\leq 5/10$, the NRI is determined from Table 1.
4. For daytime when the cloud cover is $> 5/10$, the NRI is first determined from Table 1, but modified as follows.
   (a) If the ceiling is < 2134 m, subtract 2.
   (b) If the ceiling is ≥ 2134 m and < 4877 m, subtract 1.
   (c) If the ceiling is ≥ 2134 m and the cloud cover is 10/10, subtract 1.
   (d) If the NRI has been reduced below 1 as a result of items a–c, set the NRI to 1.

For any altitude above the boundary-layer depth h, REEDM sets both σ_A and σ_E to a default free-atmosphere value of 0.0175 rad (1°). At lower altitudes, the model first computes σ_A and σ_E at an elevation of 10 m AGL using simple look-up tables (Bjorklund 1990). In these tables, the appropriate estimates of the turbulence parameters are found by cross-referencing against both the NRI and the 10 m wind speed. The σ_A estimates in these tables range from 0.0696 rad for light winds and NRI $= -1$ to 0.4538 rad for light winds and NRI $= 4$. The corresponding range of σ_E is from 0.0524 to 0.1518 rad. According to Bjorklund (1990), the REEDM look-up tables were derived from various data sources, including data from the White Sands Missile Range, New Mexico (Swanson and Cramer 1965); from the Round Hill Field Station, Massachusetts (Cramer et al. 1966); and from data published in Lumley and Panofsky (1964).

Once the values of σ_A and σ_E are computed at 10 m, the REEDM algorithm uses power laws to adjust the estimates for altitudes z up to 100 m:

$$\sigma_A(z) = \sigma_A(z_r)\left(\frac{z}{z_r}\right)^{-m} \quad (4)$$

$$\sigma_E(z) = \sigma_E(z_r)\left(\frac{z}{z_r}\right)^{n} \quad (5)$$

Here, z_r is the reference height of 10 m and the powers m and n have their own look-up tables based on the NRI and wind speed (Bjorklund 1990). These power laws come from the same data sources mentioned in the foregoing paragraph.

For altitudes above 100 m but less than h, REEDM's computations depend on atmospheric stability. The model's concept of stability is based on the well-known Pasquill (1961) stability categories, which are obtained from the NRI and the wind speed. Under convective conditions, REEDM first uses the power-law estimates of σ_A and σ_E at 100 m to compute values of σ_v and σ_w from Eqs. (1) and (2); the value of $\overline{U}$ at 100 m is interpolated from measured wind profiles (usually rawinsonde profiles). From 100 m to $0.8h$, σ_v and σ_w are assumed to be constant with height. Thus, the values of σ_A and σ_E at these heights are obtained from Eqs. (1) and (2) by using the constant values of σ_v and σ_w together with interpolated values of $\overline{U}$. In the top 20% of the boundary layer, σ_A and σ_E are linearly reduced from their values at $0.8h$ to the free-atmosphere value of 0.0175 rad.

In stable and near-neutral conditions, REEDM uses a simpler approach for estimating σ_A and σ_E above 100 m. First, Eqs. (4) and (5) are used to compute σ_A and σ_E at 100 m. A linear reduction with height is then assumed between 100 m and the boundary-layer depth h. Both σ_A and σ_E are assumed to equal 0.0175 rad at h.

REEDM performs some additional manipulations of the turbulence parameters before arriving at final values that are used to diffuse the exhaust clouds (Bjorklund 1990). For example, the turbulence parameters may be adjusted to account for the gravitational settling of large acid droplets. Also, some versions of REEDM adjusted the turbulence parameters to account for the time required for the buoyant exhaust cloud to rise to its stabilization height, an adjustment that was questioned in Eckman et al. (1996). These types of adjustments are not considered here, because they are related to the properties of the exhaust clouds and not to the basic boundary-layer turbulence structure.

4. Spatial Variability of the Turbulence at Cape Canaveral

A basic assumption in REEDM is that a single wind and turbulence profile is representative for the entire model domain. Given the variability of surface types in Fig. 1, this would appear to be a rather poor assumption for Cape Canaveral. This section investigates the spatial variability of the Cape boundary layer structure.

4.1. Aircraft Measurements

The main spatial variations near the Cape are expected to be between the land and sea. The turbulence over the Indian and Banana Rivers may also have different characteristics. Figure 4 is an example of the horizontal variations observed at the Cape on 13 July 1995. The Long-EZ flew long legs perpendicular to the coast on this flight. There is some evidence of a sea breeze in these plots. During the low-level 170 m pass, the potential temperature is nearly constant at about 300 K over the sea, and then it increases gradually inland. The easterly wind starts out at 2–3 $\mathrm{m\,s^{-1}}$ out to sea and then reaches a maximum of 6 $\mathrm{m\,s^{-1}}$ about 5 km inland. The turbulent kinetic energy e is low over the water, increases to a maximum about 10–30 km inland, and then decreases again. During the 1580 m pass, the variables showed less spatial variability. However, the reduced speed of the easterly wind at this level may be an indication of a return flow.

An important point in Fig. 4 is that conditions do not change abruptly at the coast. Rather, the variables tend to change more gradually over many kilometers. For REEDM, this means that much of the model domain will occupy the transition zone between typical conditions over the sea and conditions inland over Florida. REEDM's assumption that the turbulence is horizontally uniform will therefore often be invalid.

Figure 5 shows another example of spatial variability. In this case, the plots are mean vertical profiles for inland, sea, and Indian River flight legs from Long-EZ Flight 2 on 2 November 1995 (Session 2). This was a period when the near-surface wind was from the south-southeast. The potential-temperature profiles for all three flight legs are similar above about 1000 m. The sea data, however, indicate that a low-level inversion exists at 200–300 m. This inversion coincides with a sharp decrease in the specific humidity. In contrast, the inland potential-temperature and humidity profiles suggest well-mixed conditions at least up to 1000 m. Based on the Long-EZ profiles (including unshown data with greater vertical resolution), the mixing depth h is estimated to be about 1250 m over the land and 230 m over the sea. Such a large variation in mixing depth will of course have a significant influence on exhaust-cloud dispersion, but REEDM currently cannot account for such variations.

The Indian River data in Fig. 5 are in many respects intermediate between the inland and sea data. The potential temperature is not constant with height as with the inland data, but no obvious low-level inversion is present. Similarly, the Indian River and sea specific humidities are similar below about 200 m, but above this altitude the Indian River and inland humidities tend to converge. Wind speed over both the Indian River and the sea are higher than inland.

Figure 6 shows profiles of the velocity standard deviations for the same period as Fig. 5. The lateral σ_v and vertical σ_w standard deviations have already been introduced; σ_u is the standard deviation of the along-wind velocity component. For all three components, the inland values tend to be 2–3 times larger than the sea values. As with the mean profiles, the Indian River profiles fall between the others.

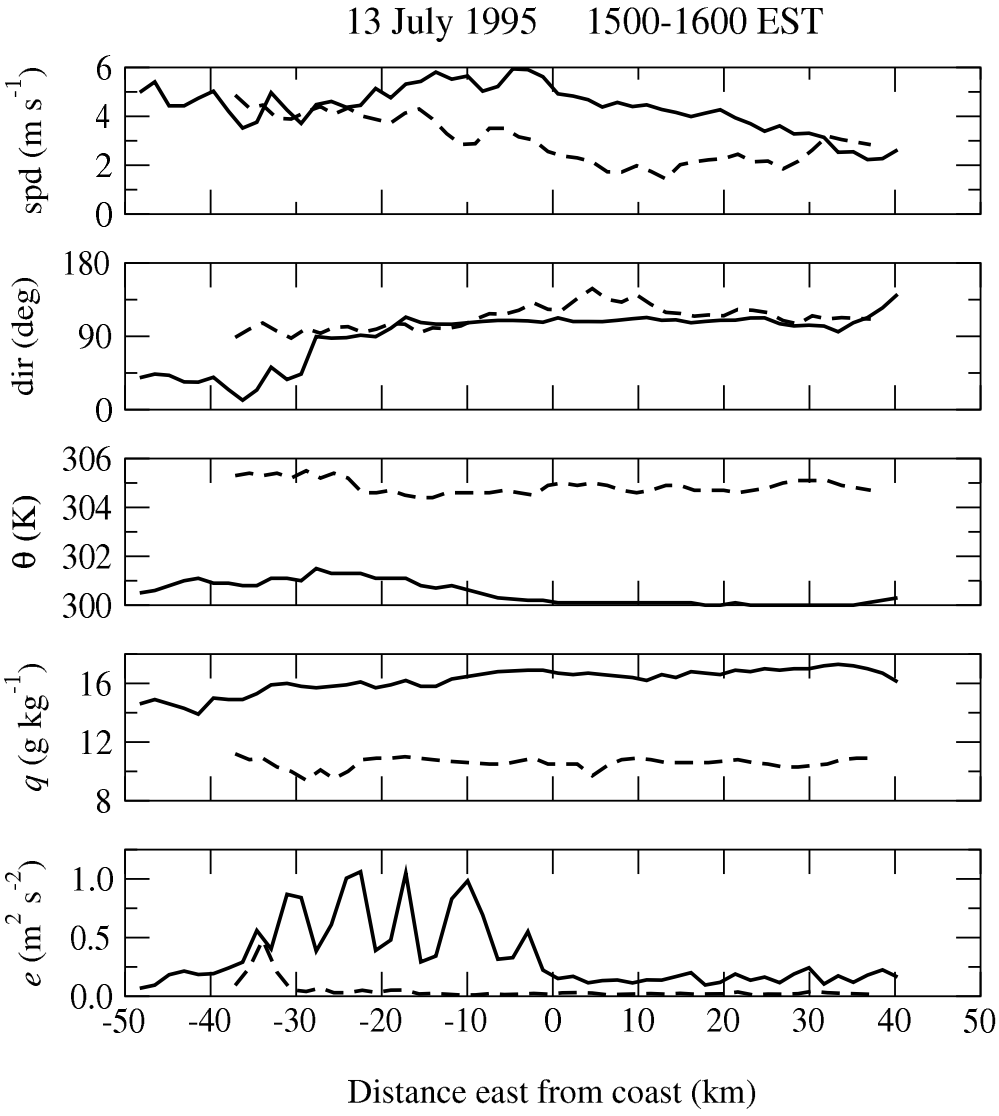

Figure 4: Meteorological conditions observed by the Long-EZ on 13 July 1995 while flying nearly perpendicular to the coast. From the top, the measurements are wind speed and direction, potential temperature θ, specific humidity q, and turbulent kinetic energy e. The solid curve was collected at an altitude of 170 m MSL, and the dashed line was at 1590 m MSL. All variables were computed using 30 s averages.

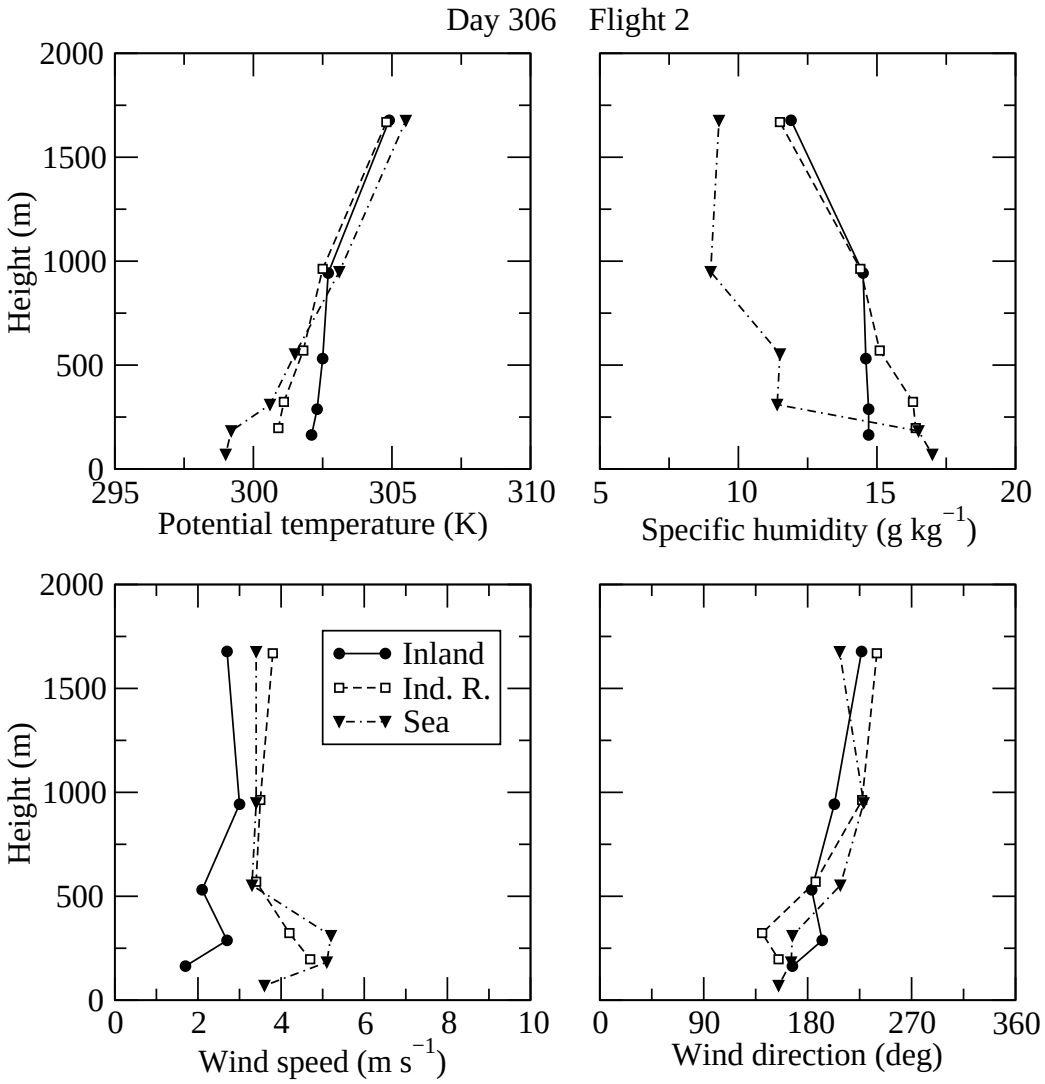

Figure 5: Mean profiles for inland, Indian River, and sea flight legs during the afternoon of 2 November 1995 (Julian Day 306). The data cover the period from 1446 to 1647 EST.

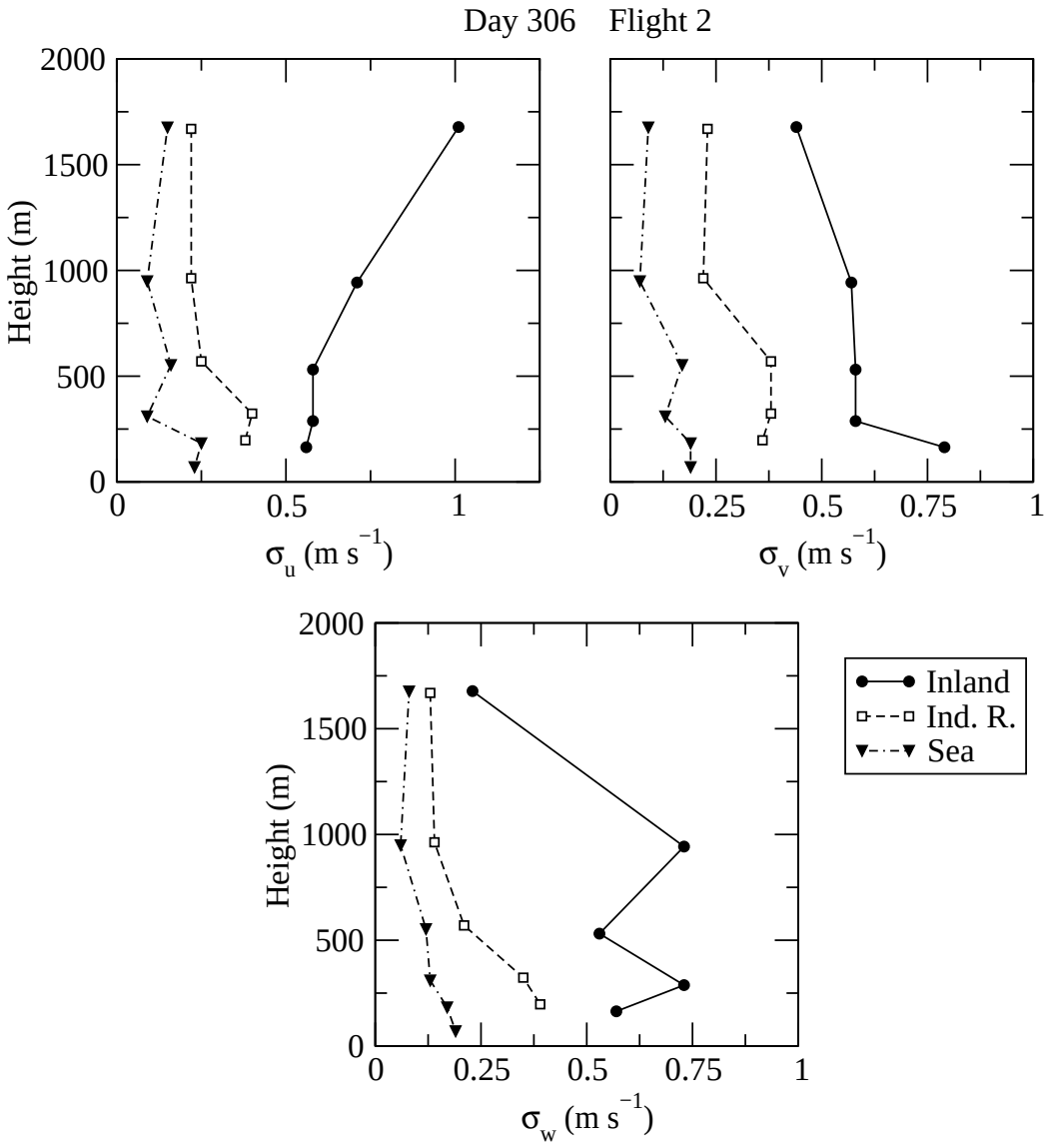

Figure 6: Turbulence profiles for inland, Indian River, and sea flight legs during the afternoon of 2 November 1995. All estimates are based on 60 s averages.

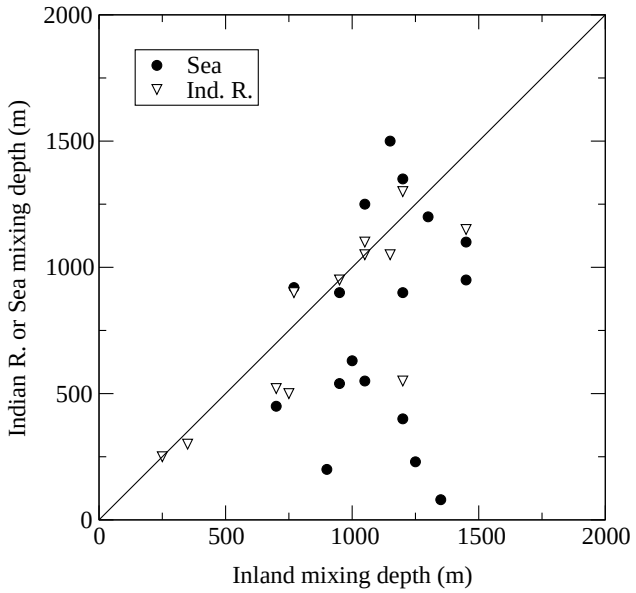

Figure 7: Observed inland mixing depths versus Indian River and sea mixing depths. All available flights from MVP Sessions 2 and 3 are included.

One complicating factor in interpreting Figs. 5 and 6 is that the profiles are not simultaneous in time. The collection periods for the inland, Indian River and sea data were respectively 1445–1514 EST, 1520–1550 EST, and 1610–1650 EST. This makes it difficult to determine how much of the observed differences are due to spatial variability and to temporal variability. The large thermal mass of the sea means that the temporal variability for the sea data is likely to be minor. For the inland and Indian River data, however, the roughly half-hour separation in time may have some influence on the observed profiles.

Although the sea mixing depth h was much smaller than the inland h on 2 November 1995, this was not always true during MVP. Figure 7 compares the estimated Indian River and sea h values with the inland values for all available flights in MVP Sessions 2 and 3. The number of data points in the figure is much smaller than the total number of flights, since the aircraft did not always fly every flight leg, and sometimes it was difficult to estimate a mixing depth from the profiles. Generally, the sea h values are smaller than the inland values, but the scatter is large. The Indian River mixing depths tend to follow the inland values better.

4.2. Sonic Anemometer Measurements

One drawback of relying solely on measurements from a single aircraft is that there is always a time lag between measurements taken at different locations. This sometimes makes it difficult to establish whether observed differences are due to spatial or temporal variations. Also, aircraft have limited endurance, so data are generally available over relatively limited time periods. These are areas where continuous tower measurements have

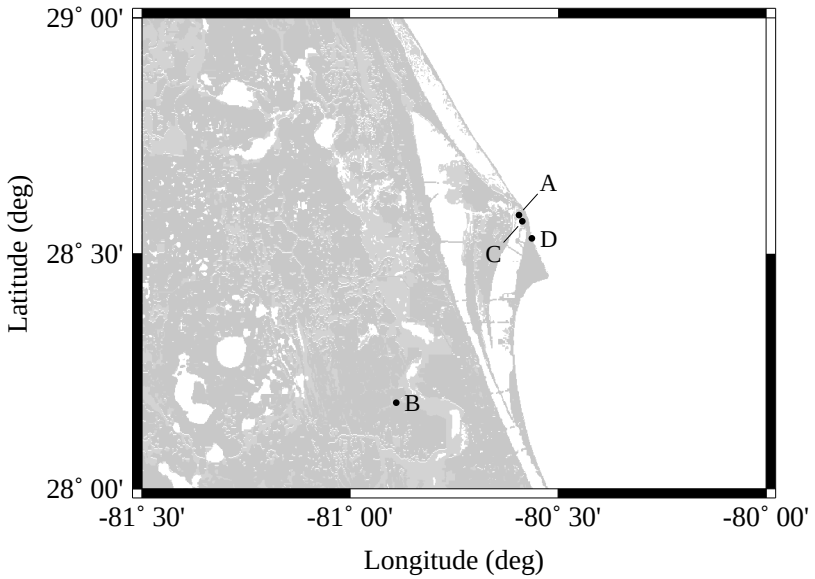

Figure 8: Positions of sonic anemometers deployed during MVP Session 2. Sonics A, B and D were on 4 m towers, whereas sonic C was located at 50 m AGL on a taller tower.

an advantage over aircraft measurements. During the MVP sessions at Cape Canaveral, the NOAA Atmospheric Turbulence and Diffusion Division (ATDD) operated a series of sonic anemometers on short towers. These were placed in various locations representing different types of terrain, and they operated continuously.

The sonic data can be used to investigate the spatial variability of the near-surface turbulence at Cape Canaveral. Here, the focus will be on the sonic data from Session 2, because the anemometers were spread over a greater variety of surface types during this session. ATDD operated four sonic anemometers during Session 2 (Fig. 8), three being located on 4 m towers and one on a taller tower.

One system (Sonic D) was located near the coast at latitude $28^\circ\,32'$. This was close to the location where surface releases of SF_6 tracer were performed during MVP. Sonic A was placed in a marshy area on the northern end of the Banana River. The local surface at this site was somewhat wetter than at Sonic D, and it was also a little further inland from the coast. A third sonic (Sonic B) was placed much further inland on a ranch about 25 km northwest of Melbourne. These systems operated more or less continuously from 27 October to 16 November 1995.

Each sonic reported measurements of the velocity standard deviations σ_u, σ_v, and σ_w using a 30-minute sampling time. To investigate the differences in turbulence characteristics among the sites, a quantity similar to the mean fractional bias (*e.g.*, Irwin and Smith 1984;

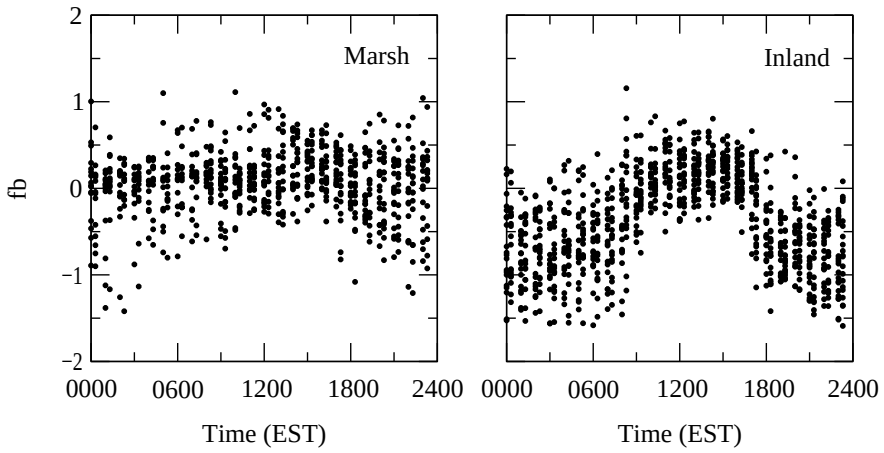

Figure 9: The fractional bias fb for σ_v plotted as a function of time. The left plot compares Sonics A and D, and the right plot compares Sonics B and D.

Tangirala et al. 1992; Eckman 1994b) will be used. Suppose that one of the three velocity standard deviations is measured at two sonics i and j during the same 30-minute period. If the observed values are denoted by O_i and O_j, the fractional bias

$$fb = 2\,\frac{O_j - O_i}{O_j + O_i} \tag{6}$$

can be used to represent the relative difference between the observations. This is basically the ratio of the difference between the two observations to their mean value. It can vary from -2 to $+2$ (assuming O_i and O_j are always positive), with a value of zero representing no difference between the pair and a value of ± 2 representing a maximum difference. Equation (6) is defined for a single pair of observations, but mean or median values of fb can be obtained when many pairs are available.

fb is positive when O_j is larger than O_i and negative when O_i is larger (assuming both measurements are positive). Sonic i can therefore be considered the "reference" site, because the sign of fb is related to whether the Sonic j observation is smaller or larger than the reference. For the MVP measurements, Sonic D is used as the reference, because it was near the location used for the SF_6 releases and is close to the rocket launch pads.

Figure 9 shows the values of fb computed from the sonic σ_v measurements [with the Sonic D observations representing O_i in Eq. (6)]. The data are plotted as a function of local time, using all available Session 2 observations. The plot for Sonics A and D is relatively constant throughout the day. The turbulence at these sites therefore tends to follow a similar diurnal pattern. The mean fb for these sites is 0.061, and the median is 0.092. Using a bootstrap resampling technique (Efron and Tibshirani 1993; Hanna 1989) with 500 resamples, the 95% confidence interval for the mean fb is 0.034 to 0.087; the corresponding confidence interval for the median is 0.073 to 0.11. The mean and median are thus different from zero at the 95% confidence level. It can be concluded that the value

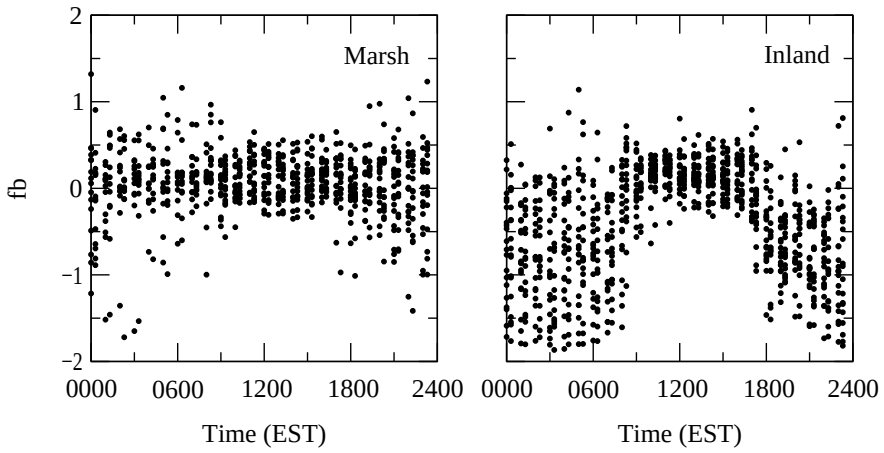

Figure 10: Same as Fig. 9, but for σ_w.

of σ_v from Sonic A is on average about 5–10% larger than that at Sonic D. This probably results from Sonic A being somewhat further inland than D.

The pattern in Fig. 9 for Sonics B and D is markedly different. A strong diurnal cycle is present, with Sonic B tending to have somewhat larger values of σ_v during the day (*i.e.*, $fb > 0$) and much smaller values ($fb < 0$) at night. Typically, the σ_v values at Sonic B are about 25–30% larger than those at Sonic D during the day. At night, the Sonic B values are only about one-third as large as those at Sonic D. Strong surface heating over the land areas of Florida leads to higher turbulence values at Sonic B during the day. A plausible explanation for the nighttime pattern is that the nearby ocean keeps a strongly stable boundary layer from developing at Sonic D, so the turbulence levels are higher.

Figure 10 shows the diurnal variations of fb using the sonic σ_w data. The patterns are similar to what are observed with σ_v. For the Sonic A and D comparison, the mean fb is 0.060 and the median is 0.098. Hence, the Sonic A values tend to run about 5–10% greater than the Sonic D values, just like σ_v.

Overall, the sonic data demonstrate that the turbulence levels can vary quite markedly from one location to another at the Cape. Sonics A and B are both strongly affected by the nearby ocean and therefore have similar turbulence characteristics. Sonic B, in contrast, has significantly different turbulence characteristics. For launch operations at the Cape, this means a single turbulence measurement near the launch pads at the coast cannot be assumed to be representative of conditions further inland.

5. Evaluation of REEDM Turbulence Algorithm

In this section, the REEDM climatological turbulence algorithm is evaluated using the Long-EZ measurements. The Long-EZ data were processed as described in Section 2. For

each available measurement of σ_A and σ_E from the aircraft, a corresponding estimate was made with the REEDM algorithm as described in Section 3. The algorithm requires estimates of solar elevation, cloud cover, cloud ceiling, near-surface wind speed, and the mixing depth. Solar elevation is readily computed. The other four must be observed. Cloud cover, ceiling, and wind speed are available on an hourly basis from the official weather reporting station at Cape Canaveral Air Station (station identifier XMR). These data were archived in a format called DATSAV2 (USAFETAC 1986). For the period of MVP Session 2, the XMR data were already available in the MVP data archive. The XMR data for Session 3 were obtained from the NOAA National Climatic Data Center.

The boundary-layer depth h was estimated by manual inspection of the vertical profiles obtained from the Long-EZ. Potential temperature and specific humidity were the main indicators used for the estimates, although wind speed and direction were also used. In stable conditions, the turbulent kinetic energy profiles were sometimes useful in estimating h. In cases when h could not be discerned from the Long-EZ data, available rawinsonde soundings were used instead.

For convective boundary layers, the REEDM algorithm also requires wind-speed profiles for turbulence estimates above 100 m AGL. As mentioned in the Introduction, there are a couple of possible data sources for the wind profiles. First, the wind profiles can be obtained from the Long-EZ. Second, rawinsonde profiles can be used. In theory, the Long-EZ profiles should result in better performance, because the wind profiles are then co-located in space and time with the turbulence measurements. However, the rawinsonde profiles are more representative of what is available operationally. Here, the REEDM algorithm is tested using both sources.

To evaluate the performance of the REEDM algorithm, the same normalized bias given in Eq. (6) will be used. If O is a single aircraft observation of σ_A or σ_E and P is the corresponding model estimate (*i.e.*, the model "prediction"), then fb is defined as

$$fb = 2\,\frac{P - O}{P + O}\,. \tag{7}$$

A total of n individual observations of fb will be available for a specified set of conditions. The primary statistics of interest for this sample of size n will be the mean $\overline{fb}$ and median $\widetilde{fb}$. These statistics give an indication of whether the model tends to have an overall bias in one direction or the other. Small values of $\overline{fb}$ and $\widetilde{fb}$ are numerically equivalent to the percentage deviation of the model from the observations. A value of 0.05, for example, means the model overestimates by about 5%. This relation does not hold with larger values; a value of 0.67 means P is twice as large as O (rather than 67% larger). For positive O and P, fb falls in the range $-2 \le fb \le 2$; this is simply a mathematical representation of the statement that the difference between two positive numbers cannot exceed twice their average.

The mean $\overline{fb}$ and median $\widetilde{fb}$ are measures of the central tendency of the fb distribution. In some cases there will also be interest in the dispersion of the distribution about the center. The two statistics that will be used for this purpose here are the sample standard deviation

Σ_{fb} and the median absolute deviation MAD_{fb}. The standard deviation is well known, and MAD_{fb} is defined as

$$MAD_{fb} = 1.4826\,\text{median}\{|fb - \widetilde{fb}|\}\,. \tag{8}$$

The constant 1.4826 is used so that $MAD_{fb} \approx \Sigma_{fb}$ for normal distributions and large sample sizes. (Of course, there is no expectation that $MAD_{fb} \approx \Sigma_{fb}$ when these conditions are not met.) Like $\widetilde{fb}$, MAD_{fb} has the advantages that it is nonparametric and less affected by outliers.

Since $\overline{fb}$ and $\widetilde{fb}$ are sample statistics, they may deviate significantly from the underlying population mean $\overline{\mu}$ and median $\widetilde{\mu}$. These sample statistics are therefore incomplete unless additional information is provided on their expected variability from one sample to another. The approach taken here is to use the bootstrap resampling technique (Efron and Tibshirani 1993; Hanna 1989) to estimate standard deviations for $\overline{fb}$ and $\widetilde{fb}$. Taking $\widetilde{fb}$ as an example, the bootstrap method can be used to estimate the standard deviation $s_{\widetilde{fb}}$ of $\widetilde{fb}$. A $(1-\alpha)100\%$ confidence interval for the population median $\widetilde{\mu}$ can then be estimated as (*e.g.*, Hanna 1989)

$$\widetilde{fb} - t_{\alpha/2}\, s_{\widetilde{fb}} < \widetilde{\mu} < \widetilde{fb} + t_{\alpha/2}\, s_{\widetilde{fb}}\,, \tag{9}$$

where $t_{a/2}$ is the t distribution with $\nu = n - 1$ degrees of freedom and α is the significance level of the test. n is number of observations in the original sample, not the number of bootstrap resamples.

Bootstrap estimates can also be used to put a confidence interval on the difference $\widetilde{\mu}_i - \widetilde{\mu}_j$ between the population medians from two treatments i and j. The difference $\widetilde{fb}_i - \widetilde{fb}_j$ will serve as a point estimator of $\widetilde{\mu}_i - \widetilde{\mu}_j$. The variance of $\widetilde{fb}_i - \widetilde{fb}_j$ can be estimated as $s^2_{\widetilde{fb};i} + s^2_{\widetilde{fb};j}$, where $s_{\widetilde{fb};i}$ and $s_{\widetilde{fb};j}$ are the standard deviations of $\widetilde{fb}_i$ and $\widetilde{fb}_j$ obtained from the bootstrap procedure. A confidence interval for the difference is then

$$(\widetilde{fb}_i - \widetilde{fb}_j) - t_{\alpha/2}\sqrt{s^2_{\widetilde{fb};i} + s^2_{\widetilde{fb};j}} < \widetilde{\mu}_i - \widetilde{\mu}_j < (\widetilde{fb}_i - \widetilde{fb}_j) + t_{\alpha/2}\sqrt{s^2_{\widetilde{fb};i} + s^2_{\widetilde{fb};j}}\,. \tag{10}$$

The degrees of freedom ν for the t distribution are a weighted average based on the values ν_i and ν_j for each treatment:

$$\nu = \frac{\left(s^2_{\widetilde{fb};i} + s^2_{\widetilde{fb};j}\right)^2}{s^4_{\widetilde{fb};i}/\nu_i + s^4_{\widetilde{fb};j}/\nu_j}\,. \tag{11}$$

Equations (10) and (11) are essentially the same as those used for the difference between two means (Walpole and Meyers 1978; Sachs 1984). They are based on the assumption that the bootstrap estimates of $\widetilde{fb}$ for each treatment are approximately normally distributed.

There are, of course, caveats associated with applying Eqs. (9)–(11) to atmospheric measurements. The statistical theory assumes all the data are independent. (Such an assumption is used in nearly all standard statistical procedures.) This assumption is difficult and usually impractical to fulfill in field measurements, because atmospheric motions retain some correlation over long periods of time. The values of fb collected during a single Long-EZ flight, for example, will exhibit some correlation depending on the

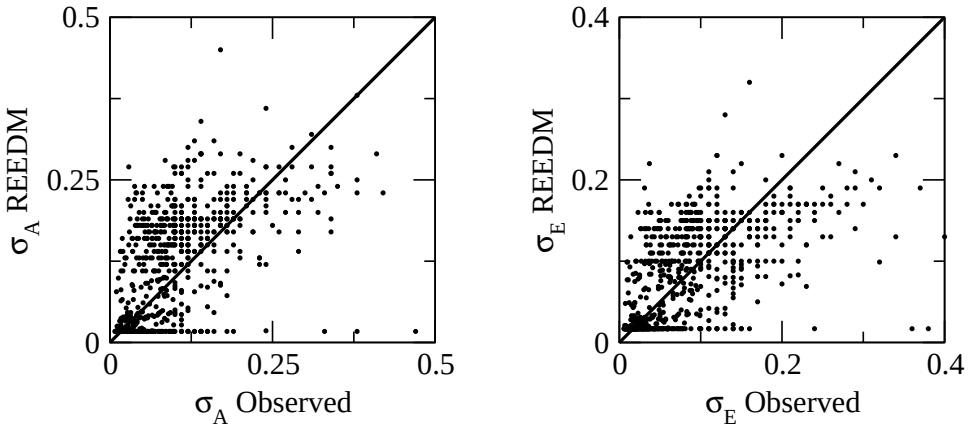

Figure 11: Scatter plots for the aircraft observations and REEDM estimates of σ_A and σ_E. A small number of data points are located outside the bounds of each plot.

separation in both time and space. As discussed by Hanna (1989), this dependence effectively reduces the degrees of freedom ν below the nominal value of $n-1$. The value $n-1$ can therefore be considered to be an upper bound on ν. A lower bound on ν can be obtained by assuming the observations are independent only if they come from different aircraft flights. ν would then equal $k-1$, with k being the number of separate flights. The effective value of ν falls somewhere between $k-1$ and $n-1$.

5.1. Evaluation Using Aircraft Wind Profiles

The first comparison uses the Long-EZ wind profiles as input to the REEDM algorithm. This represents a "best case" scenario, since the mean wind speed $\overline{U}$ used as input to the algorithm comes from the same time and location as the aircraft σ_A and σ_E measurements. Errors due to spatial variations in the mean winds and to using wind profiles that are possibly hours old should be minimized in this comparison. In all, 781 pairs of aircraft measurements and REEDM estimates were available from the MVP Sessions.

Scatter plots for all the paired observations and model estimates are shown in Fig. 11. The scatter for both σ_A and σ_E is quite large. Also, REEDM appears to overestimate the turbulence on the left sides of the plots and to somewhat underestimate on the right sides. The horizontal rows of data points along the bottoms of the plots are cases when REEDM went to its default value of 1° above the boundary layer. The median value of the observed σ_A for all the data is 0.082 rad, whereas the median REEDM estimate is 0.12 rad. For σ_E, the median observed and estimated values are 0.072 and 0.086 rad.

Figure 11 is useful as a general overview of the REEDM performance, but the data points cover a wide range of altitudes, surface types, and stabilities. In a statistical sense, these various conditions can be considered to be different treatments applied to the turbulence data. However, unlike textbook statistics in which the experimenter has control over the treatments applied to the individual samples, the treatments for the MVP turbulence data

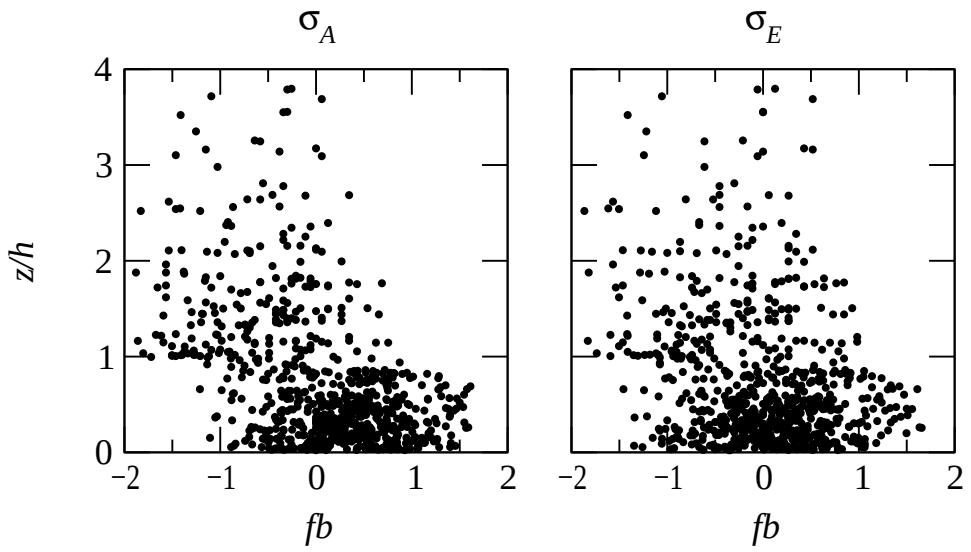

Figure 12: The fractional bias fb as a function of height. A few data points are above the upper bound of the plot.

are at the mercy of external factors such as the weather and the scheduling of the MVP tracer releases.

To further investigate the performance of the REEDM turbulence algorithm, the three major treatments will be considered to be altitude z, surface type, and the stability class. For the altitude, the measurements will be separated according to whether they are above or below the boundary-layer depth h. Surface type will fall into the five categories (inland, sea, Indian River, Banana River, and Merritt Island) discussed in Section 2. Stability will be grouped into the A, B, C, D, and E categories of Pasquill (1961). Category A is highly unstable, D is neutral, and E is stable. REEDM uses one algorithm when the boundary layer is unstable (categories A–C) and another for neutral and stable conditions (Bjorklund 1990). The surface-type and stability class are only considered for measurements within the boundary layer, since they by definition should have no effect in the free troposphere above.

In considering the altitude, one question is whether there is a systematic difference in REEDM performance with height. Figure 12 shows fb plotted as a function of the ratio z/h. The plot for σ_A clearly shows a tendency for fb to be greater than zero within the boundary layer and to be negative above the boundary layer. A similar but less distinct pattern is present for σ_E. The distributions in this figure indicate that most of the REEDM overestimates seen in Fig. 11 are associated with altitudes within the boundary layer, whereas most of the underestimates are at altitudes above the boundary layer.

Table 2 provides sample statistics for the 215 observations that were collected above the estimated boundary-layer depth. Standard deviations are provided for some statistics, based on the bootstrap technique with 500 resamples. As can be seen from the table, REEDM always defaults to $\sigma_A = \sigma_E = 0.017\,\mathrm{rad}$ (*i.e.*, 1°) above the boundary layer, but the observations are 40–75% larger. This could be due to errors in the estimates of the

Table 2: MVP sample statistics for $z > h$. In column 1, O is an aircraft observation of σ_A or σ_E, and P is the corresponding REEDM estimate. Means are denoted by an overbar and medians by a tilde. For statistics followed by a ± symbol, the number after the symbol is the estimated standard deviation for the statistic. These standard deviations are based on a bootstrap resampling technique with 500 resamples.

statistic	σ_A	σ_E
n	215	215
$\overline{O}$	0.051±0.004	0.041±0.004
$\overline{P}$	0.017	0.017
$\widetilde{O}$	0.030±0.003	0.024±0.002
$\widetilde{P}$	0.017	0.017
$\overline{fb}$	-0.61±0.04	-0.40±0.04
$\widetilde{fb}$	-0.55±0.08	-0.34±0.09
Σ_{fb}	0.59	0.66
MAD_{fb}	0.66	0.75

boundary-layer depth h. If h is systematically underestimated, the model estimates would be too small for altitudes between the estimated and true values of h. However, it is expected that underestimates in h would cause fb in Fig. 12 to trend towards zero for $z \gg h$; such a pattern is not evident. Another possibility is simply that the default turbulence level used in REEDM is too small. If this is true, Table 2 indicates that 0.025–0.030 rad may be more representative for σ_A and σ_E in the free troposphere than 0.017 rad. A third possibility is that the Long-EZ turbulence observations are artificially inflated by noise in the data acquisition system; such noise contamination would be more significant in the light turbulence observed above the boundary layer.

In moving on to the evaluation of the REEDM algorithm for $z \leq h$, consideration must be given to the effects of the surface type and stability. There are 566 Long-EZ observations that fall within the estimated boundary layer depth. Table 3 shows how these observations are spread over the surface types and stabilities. About 44% of the observations come from the inland surface. Comparatively few observations are available for the Banana River and Merritt Island surfaces, because these flight legs were only flown on certain days during Session 3. Table 3 also shows the number of individual flights involved in each surface type and stability.

Table 4 shows how the median $\widetilde{fb}$ varies with surface type and stability for σ_A. The corresponding statistics for σ_E are given in Table 5. Bootstrap estimates of $s_{\widetilde{fb}}$ are also provided in each table.

In considering statistical results such as those given in Tables 4 and 5, a common first step is to determine whether the various treatments (*i.e.*, surface types and stabilities) produce

Table 3: Number of observations and flights in each surface type and stability for $z/h < 1$. The numbers are presented as n:k, where n is the number of observations and k is the number of flights.

	Surface					
Stability	Banana River	Inland	Merritt Island	Indian River	Sea	Total
A	6:2	0:0	7:1	0:0	0:0	13:2
B	28:5	51:10	32:6	16:5	16:5	143:15
C	5:2	88:18	5:1	39:10	31:10	168:27
D	1:1	68:16	0:0	38:11	67:15	174:25
E	5:1	41:5	0:0	19:4	3:1	68:7
Total	45:7	248:38	44:6	112:25	117:27	566:45

significantly different results. An analysis of variance is often used for this purpose. However, analysis of variance requires that the underlying populations for all the treatments are normally distributed and have the same variance. Since fb must fall in the range from -2 to $+2$, it is not clear that it will necessarily be normally distributed. The null hypothesis that all the treatments have the same population variance is commonly tested using Bartlett's test. This test produces a test statistic of $\chi^2 = 86$ for the σ_A data in Table 4 and $\chi^2 = 72$ for the σ_E data in Table 5. The null hypothesis of equal variances is tested by comparing χ^2 with a chi-square distribution. With 18 degrees of freedom and a 95% confidence coefficient, the chi-square distribution has a value of 29. The treatments thus do not have equal population variances according to this test. A standard analysis of variance is therefore not appropriate.

A nonparametric alternative to the standard analysis of variance is the H test (Kruskal and Wallis 1952; Sachs 1984). It does not require equal population variances or that the data are normally distributed. The test is based on sorting n data points in ascending order and then assigning each point a rank from 1 to n. The null hypothesis that all the data come from identical populations is rejected if the test statistic H exceeds a chi-square value with $m - 1$ degrees of freedom, where m is the number of treatments. For the fb data, this test gives $H = 245$ for σ_A and $H = 220$ for σ_E. Both of these are well above the chi-square value of 29 for a 95% confidence coefficient. The H test therefore indicates that some of the differences observed in Tables 4 and 5 represent real differences in the underlying populations.

To evaluate the REEDM algorithm's performance, the values of $\widetilde{fb}$ in Tables 4 and 5 are used to determine whether the algorithm is over- or underestimating the turbulence parameters. The bootstrap standard deviations $s_{\widetilde{fb}}$ can be used to put a confidence interval on the population medians $\widetilde{\mu}$ and the differences $\widetilde{\mu}_i - \widetilde{\mu}_j$, as in Eqs. (9) and (10). As discussed above, the effective degrees of freedom ν_i for treatment i is likely to lie between $k_i - 1$ and $n_i - 1$, with k_i and n_i respectively being the number of flights and observations available for the treatment.

Table 4: $\widetilde{fb}$ computed from σ_A for each surface type and stability class. The data are only for $z/h < 1$.

	Surface				
Stability	Banana River	Inland	Merritt Island	Indian River	Sea
A	0.89 ± 0.28	—	0.00 ± 0.26	—	—
B	0.73 ± 0.02	-0.13 ± 0.06	0.23 ± 0.06	0.72 ± 0.07	0.94 ± 0.22
C	0.53 ± 0.06	0.25 ± 0.04	0.30 ± 0.17	0.63 ± 0.09	1.02 ± 0.16
D	—	0.07 ± 0.07	—	0.46 ± 0.07	0.65 ± 0.12
E	-0.44 ± 0.45	-0.04 ± 0.11	—	-0.35 ± 0.09	-1.03 ± 0.25
All	0.72 ± 0.03	0.06 ± 0.02	0.19 ± 0.06	0.48 ± 0.05	0.79 ± 0.07

Table 5: Same as Table 4, but for σ_E.

	Surface				
Stability	Banana River	Inland	Merritt Island	Indian River	Sea
A	0.48 ± 0.29	—	-0.55 ± 0.24	—	—
B	0.62 ± 0.03	-0.42 ± 0.06	-0.11 ± 0.07	0.39 ± 0.10	0.65 ± 0.28
C	0.31 ± 0.09	0.08 ± 0.05	0.00 ± 0.10	0.45 ± 0.08	0.77 ± 0.18
D	—	-0.24 ± 0.08	—	0.24 ± 0.11	0.51 ± 0.11
E	-0.57 ± 0.67	0.04 ± 0.08	—	-0.22 ± 0.12	-1.21 ± 0.33
All	0.53 ± 0.06	-0.13 ± 0.04	-0.11 ± 0.07	0.33 ± 0.05	0.55 ± 0.08

In Tables 4 and 5, the last row contains summary statistics for all the stability classes. For σ_A, the inland surface is seen to have the smallest overall bias. Equation (9) gives $0.02 < \tilde{\mu} < 0.10$ for this case, given the more conservative $\nu = k - 1$ and a 95% confidence coefficient. The sea surface has the worst performance for σ_A, with $0.65 < \tilde{\mu} < 0.93$. This makes sense, given that the REEDM algorithm is based on data collected over land. The other surface types tend to fall between the inland and sea surfaces. The pattern observed for the last row in Table 5 is similar to that for σ_A, except that each median is shifted downward by roughly 0.2. For the σ_E values over land, the 95% confidence interval for the median is $-0.21 < \tilde{\mu} < -0.05$, and for the sea it is $0.39 < \tilde{\mu} < 0.71$.

The summary rows in Tables 4 and 5 indicate that the REEDM algorithm has a relatively small overall bias over land and a large positive bias over the sea. The REEDM estimates of σ_A over the sea were typically at least a factor of two greater than the observations. For σ_E, the REEDM overestimation over the sea was about 75%. Caution must be exercised, however, in drawing more detailed conclusions from the bottom rows in the two tables. The measurements for each surface type are distributed unevenly over the stability classes (Table 3), so the $\widetilde{fb}$ differences observed in the bottom rows may be partly due to stability and not surface type.

Tables 4 and 5 show that even within a single surface type, the REEDM algorithm's performance can vary strongly with stability. For inland data in Table 4, $\widetilde{fb}$ goes from -0.13 for stability class B to 0.25 for class C and then back down to -0.04 for class E. Using Eq. (9) and a 95% confidence coefficient, the -0.13 for class B is significantly different from zero using $\nu = n - 1$, but not using the more conservative $\nu = k - 1$. Neither $\widetilde{fb} = 0.07$ for class D nor $\widetilde{fb} = -0.04$ for class E are significantly different from zero. The 0.38 difference in $\widetilde{fb}$ between classes B and C is strongly significant based on Eq. (10), as is the 0.18 difference between classes C and D.

The inland statistics in Table 4 support the conclusion that the REEDM algorithm produces relatively unbiased estimates of σ_A for D and E stabilities and overestimates by about 30% for stability C. The statistical support for the underestimation in class B is weaker. To investigate these patterns further, Fig. 13 shows how fb varies with height for the four stability classes. The data for class C are near zero at small z/h, but they trend higher with height. The overestimation for this class thus appears to result from the REEDM algorithm increasing σ_A too rapidly with height. For class B, the data in the figure are consistently on the negative side at all heights. The weak underestimation for class B therefore is more related to the near-surface estimates of σ_A being too small.

The sea data in Table 4 indicate consistent overestimation except for stability class E. However, the class E $\widetilde{fb}$ has very little statistical significance since there are only three values from one flight. All three $\widetilde{fb}$ values for classes B–D are significantly different from zero but are not significantly different from each other. From these results, one can conclude that the REEDM algorithm overestimates σ_A by a factor of two or more over the sea in near-neutral and unstable conditions.

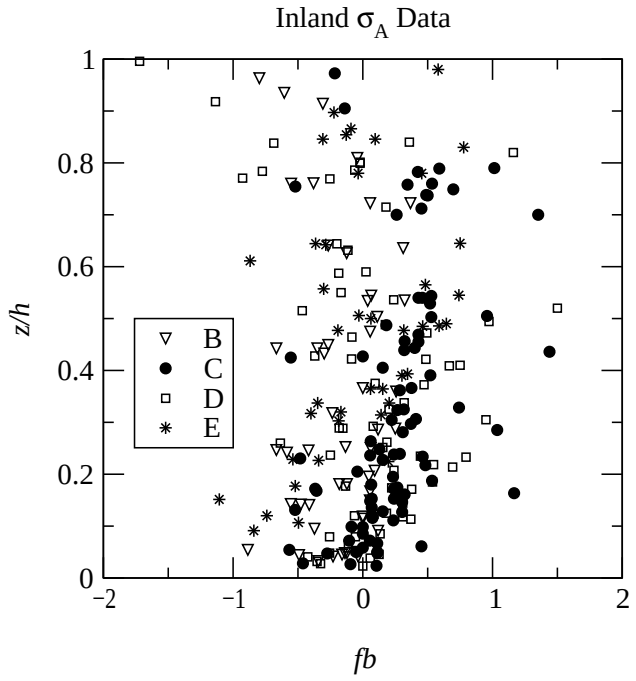

Figure 13: fb height for σ_A and the inland surface type. The four stability classes are denoted by different symbols.

The pattern of $\widetilde{fb}$ for the Indian River surface in Table 4 is similar to that for sea, but the degree of overestimation appears to be less. For stability classes B–D, the values of $\widetilde{fb}$ are all significantly different from zero, but only the difference of 0.26 between classes B and D is significant. The value of -0.35 for class E produces a 95% confidence interval of $-0.64 < \tilde{\mu} < -0.06$ using the lower-limit of $\nu = 3$. This $\widetilde{fb}$ for class E is significantly different from the class D value.

All the Indian River $\widetilde{fb}$ values are significantly different from the corresponding inland values, although for class E the difference is only significant using the upper ν limits based on n. In comparing Indian River and sea, only the difference between the class C values is statistically significant. The REEDM algorithm therefore appears to overestimate the values of σ_A over the Indian River in near-neutral and unstable conditions, as is the case over the sea. This overestimation is somewhat less than that for the sea (at least for class C). Still, the estimated values of σ_A are typically high by nearly a factor of two.

For the Banana River and Merritt Island surfaces, only stability class B has significant sample sizes. The Banana River data are statistically not different from the sea and Indian River data for this stability. The Banana River is close enough to the coast that the values of σ_A are similar to what is observed over the sea. Merritt Island is a land surface and is therefore expected to have some similarity to the inland surface. However, its value of $\widetilde{fb} = 0.23$ for stability B is significantly different from the other surfaces. Merritt Island is close enough to the coast that the observed values of σ_A are somewhere between the inland inland values and the values observed over the three water surfaces.

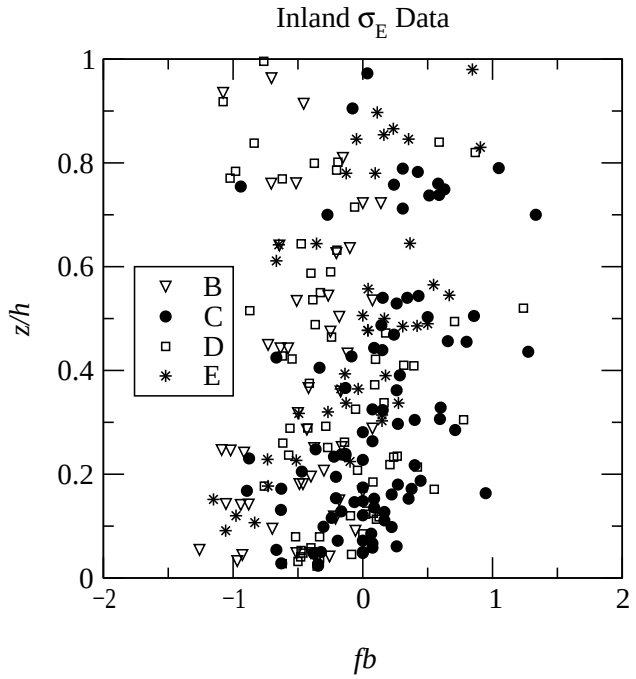

Figure 14: Same as Fig. 13, but for σ_E.

In turning now to the σ_E values of $\widetilde{fb}$ in Table 5, it is noticed that overall the relative differences follow a pattern similar to what is observed with σ_A. The individual values for each treatment are generally smaller in Table 5 than in Table 4.

For the inland surface in Table 5, there are significant negative biases for classes B and D, but no significant bias for the other two classes. Unlike the case with σ_A, the REEDM algorithm does not appear to overestimate σ_E in C stability. Figure 14 shows that the bias for class B is fairly consistent with height, suggesting that the problem lies with the near-surface estimation of σ_E. The class D bias is also fairly steady with height. The class C bias does tend to have a trend with height, but it is weaker than in Fig. 13. The low value of $\widetilde{fb}$ for this class my therefore be fortuitous in that underestimates at small z/h are balanced by overestimates at higher altitudes.

The sea values in Table 5 show a consistent level of overestimation, but the degree of overestimation is less than with σ_A. For stability classes B–D, the overestimation is close to a factor of two. Class E has too few observations to make any conclusions.

The Indian River surface typically shows overestimations around 45% for σ_E in unstable and near-neutral conditions. These values of $\widetilde{fb}$ are significantly different from zero, although the 0.24 for stability class D is only marginally significant. The -0.22 for class E is not significantly different from zero at a 95% confidence level due to the small sample size. Using Eq. (10), the Indian River σ_E values of $\widetilde{fb}$ are significantly different from the inland values but not from the sea values.

As stated above, only stability class B has significant sample sizes for the Banana River and Merritt Island surfaces. The Banana River value of 0.62 in Table 5 is significantly different from zero, and it shows a level of overestimation similar to sea. The $\widetilde{fb} = -0.11$ for Merritt Island is not significantly different from zero, but the differences between its $\widetilde{fb}$ and those for inland and sea are significant. This is consistent with the results for σ_A.

5.2. Evaluation Using Rawinsonde Wind Profiles

In this section, the REEDM turbulence estimates are based on available rawinsonde wind profiles rather than the Long-EZ profiles. This more closely replicates what is available at Cape Canaveral during launch operations. It is expected that the use of the rawinsonde data should lead to some degradation in the REEDM algorithm's performance, since the rawinsonde release point can be many kilometers away from the locations where the σ_A and σ_E measurements were taken. Also, the most recent rawinsonde may have been released hours before the time of the Long-EZ turbulence measurements. Even with these issues, the reduction in performance resulting from the use of rawinsonde winds is not expected to be major, since the need for a wind profile in REEDM's turbulence algorithm is fairly limited. As discussed in Section 3., the algorithm requires a wind profile only in convective conditions at altitudes between 100 m AGL and the boundary-layer height h. For near-neutral and stable conditions or any altitude below 100 m AGL, only a 10 m reference wind speed is required. (REEDM does use a wind profile to compute a dispersion contribution due to wind shear, but this is not part of the turbulence algorithm.)

For each Long-EZ flight, the MVP data archive was searched to find a rawinsonde sounding that took place just before the flight. Generally, the soundings were considered acceptable if they were no more than about four hours old at the time of the flight. In a couple cases, a sounding was available just after a flight started, and it was used in the computations. If a rawinsonde sounding was not available within a reasonable period before a flight, that flight was excluded from the analysis.

For the remaining Long-EZ flights with available rawinsonde data, the rawinsonde wind profiles were used in the REEDM algorithm when needed. The rawinsonde data was also used to compute the 10 m reference wind speed used in REEDM's lookup tables (see Section 3.). In Section 5.1., this reference speed was instead extracted from the station XMR data, because the Long-EZ did not fly low enough to provide a good estimate of the 10 m wind speed.

In all, 541 individual REEDM estimates of σ_A and σ_E were computed using the rawinsonde winds. Table 6 shows the fb statistics for these estimates. For comparison, the same statistics are shown for the REEDM estimates based on the Long-EZ winds. As expected, the differences between the REEDM estimates based on rawinsonde winds and Long-EZ winds in Table 6 are fairly small. The rawinsonde statistics do trend slightly higher. Both a paired t test and the Wilcoxon test for paired data (Sachs 1984) indicate that the observed differences in $\overline{fb}$ and $\widetilde{fb}$ are significant with a 95% confidence coefficient. The use

Table 6: Statistics comparing REEDM turbulence estimates based on rawinsonde winds and Long-EZ winds for $z/h < 1$.

	σ_A		σ_E	
Stat	Long-EZ	Rawin	Long-EZ	Rawin
n	541	541	541	541
$\overline{fb}$	0.29±0.02	0.35±0.02	0.11±0.02	0.18±0.03
$\widetilde{fb}$	0.30±0.03	0.34±0.04	0.10±0.03	0.15±0.03
Σ_{fb}	0.56	0.56	0.59	0.60
MAD_{fb}	0.54	0.54	0.59	0.64

Table 7: Statistics comparing REEDM turbulence estimates based on rawinsonde winds and Long-EZ winds for $z/h < 1$. Only inland flight legs are included.

	σ_A		σ_E	
Stat	Long-EZ	Rawin	Long-EZ	Rawin
n	235	235	235	235
$\overline{fb}$	0.06±0.03	0.15±0.03	-0.13±0.03	-0.01±0.04
$\widetilde{fb}$	0.06±0.02	0.13±0.04	-0.13±0.04	-0.06±0.03
Σ_{fb}	0.46	0.49	0.49	0.54
MAD_{fb}	0.39	0.44	0.44	0.48

of rawinsonde winds therefore appears to lead to a small but statistically significant increase in both $\overline{fb}$ and $\widetilde{fb}$. The effect of the rawinsonde winds on the model precision, as indicated by Σ_{fb} and MAD_{fb}, is also small.

Of course, the statistical tests performed in Section 5.1. indicated that the REEDM algorithm worked significantly better over land. The results in Table 6 may therefore be affected by the poor performance over water. Table 7 shows the statistics for the inland flight legs only. For both σ_A and σ_E, the statistics for the rawinsonde-based estimates have somewhat larger values than those based on the Long-EZ winds. For σ_E this actually leads to a somewhat lower bias for the rawinsonde estimates. However, the Long-EZ estimates appear to be slightly more precise, as measured by Σ_{fb} and MAD_{fb}.

The results in Tables 6 and 7 suggest that the rawinsonde-based estimates of σ_A and σ_E are consistently larger than those based on a combination of the Long-EZ wind profiles and XMR 10 m reference winds. One reason for this is that, on average, the stability class computed from the rawinsonde winds is slightly more unstable than that computed with the reference wind from the XMR station. This can only happen if the near-surface rawinsonde wind speed is slightly lower on average than the XMR wind speed. Another factor is that the rawinsonde wind profiles often show a local wind-speed maximum near 100 m AGL, which in convective conditions causes the REEDM algorithm to produce larger

values of σ_A and σ_E at altitudes above 100 m (see Section 3.). It is unclear whether this speed maximum is physically real or an artifact of the rawinsonde wind measurements.

6. Vertical Extrapolation of Near-Surface Turbulence Measurements

The REEDM climatological turbulence algorithm is designed for use at a location where no direct turbulence measurements are available. The turbulence estimates are thus based on a few stability classes that can be determined from easily available measurements such as wind speed, cloud cover, *etc.* Algorithms of this type are still in common use for operational purposes, although the meteorological community has increasingly advocated the use of on-site turbulence measurements for dispersion modeling (*e.g.*, Hanna et al. 1977, 1982; Irwin 1983). Turbulence instruments such as sonic anemometers and sodars have become relatively low-cost and reliable. On-site measurements have therefore become much easier to obtain than in the past.

With the MVP data archive, it is possible to test whether on-site turbulence measurements may provide significant improvements in turbulence estimates at Cape Canaveral. As was discussed in Section 4.2., the NOAA Atmospheric Turbulence and Diffusion Division operated several sonic anemometers during the MVP sessions at the Cape. These sonic anemometer turbulence measurements are in this section extrapolated upward and compared with the Long-EZ measurements.

Since direct measurements of the friction velocity u_* and the Monin-Obukhov length L are available from the sonic anemometers, it was decided to base the vertical extrapolation of the sonic turbulence measurements on standard algorithms available in the scientific literature. Different algorithms are required for different atmospheric stabilities, so the first task is to decide when the boundary layer is convective, near-neutral, and stable. Following Holtslag and Nieuwstadt (1986), this separation is based on the ratio between the boundary-layer depth h and the Monin-Obukhov length L. The boundary layer is assumed to be convective when $h/L < -5$ and stable when $h/L > 1$. Intermediate values are assumed to indicate near-neutral conditions.

Measurements have consistently indicated that the standard deviation σ_v of the lateral velocity component is nearly constant with height in the convective boundary layer (Panofsky et al. 1977; Caughey and Palmer 1979; Panofsky and Dutton 1984; Hicks 1985). The sonic measurements of σ_v were therefore used as a constant for all heights between the surface and $0.8h$. For $0.8h \leq z < h$, σ_v was reduced linearly with height, but was not allowed to go below a value $\sigma_v = 0.026\overline{U}$; this value corresponds to the assumed turbulence intensity of $\sigma_A = 1.5^\circ$ for heights above the boundary layer.

The variation of the vertical-component standard deviation σ_w in convective conditions is more complex. Within the surface layer ($z < 0.1h$), σ_w tends to increase with height (Panofsky et al. 1977; Panofsky and Dutton 1984). For these heights, the sonic

measurements are extrapolated using the equation (Panofsky et al. 1977)

$$\frac{\sigma_w}{u_*} = 1.25 \left[1 - 3\frac{z}{L}\right]^{1/3} \quad . \tag{12}$$

The sonic extrapolation actually requires only the proportionality $\sigma_w \propto (1 - 3z/L)^{1/3}$, since σ_w is already known at the height of the sonic anemometer. Above $z = 0.1h$, σ_w is assumed to behave similarly to σ_v. Specifically, it is assumed to be constant with height in the range $0.1h \leq z < 0.8h$ and to decrease linearly with height within the top 20% of the boundary layer. This structure agrees with both measurements (Caughey and Palmer 1979; Panofsky and Dutton 1984) and with modeling based on large-eddy simulations (Moeng and Sullivan 1994).

The vertical variation of the turbulence in stable conditions is based on Lenschow et al. (1988). They found that both σ_v and σ_w can be modeled with the relation

$$\sigma_v, \sigma_w \propto [1 - z/h]^{7/8} \quad . \tag{13}$$

This proportionality is used at all heights in the stable boundary layer. In near-neutral conditions, both σ_v and σ_w are assumed to be constant with height within the surface layer (Panofsky and Dutton 1984). Between $0.1h$ and h, the standard deviations are assumed to drop off linearly with height. This fits the results of Moeng and Sullivan (1994) fairly well for a shear-driven boundary layer.

For all stabilities, the σ_v and σ_w estimates were converted to σ_A and σ_E using Eqs. (1) and (2). The mean wind speed from the Long-EZ was used in these equations. The algorithms given above assume that the turbulence decreases to zero at the top of the boundary layer. An additional requirement was added to require that σ_A and σ_E be no less than 1.5°. This is the assumed turbulence level in the free troposphere above the boundary layer.

The first set of measurements to be evaluated comes from Sonic B, which was referred to in Section 4.2. and Fig. 8. This site was about 25 km northwest of Melbourne, and was in operation only during MVP Session 2. A short tower was used at the site, and the sonic anemometer was at about 4 m AGL.

Sonic B is representative of conditions well inland from the coast. Extrapolated turbulence profiles from this site are therefore compared with the Long-EZ turbulence measurements taken on the inland legs in Fig. 2. Table 8 shows the fb statistics for this comparison. Only measurements with $z/h < 1$ are included. The corresponding statistics from REEDM's climatological algorithm are also shown.

The statistics in Table 8 are based on a sample size of 111. Of these, 89 were unstable ($h/L < -5$), 22 were stable ($h/L > 1$), and none were near-neutral. The unstable and stable cases are listed separately in the table. For σ_A, the fb statistics for the sonic extrapolation are consistently smaller than those for REEDM. Using a paired t test, the 0.06 difference in $\overline{fb}$ for the σ_A unstable case is not significant with a 95% confidence coefficient, but it is significant with a 90% confidence coefficient. A Wilcoxon signed-rank

Table 8: Statistics comparing turbulence profiles based on Sonic B extrapolations with Long-EZ observations. For comparison, the statistics from the REEDM turbulence algorithm are also shown. Only Long-EZ measurements from the inland flight legs and within the boundary layer are included.

	σ_A		σ_E	
Stat	Sonic	REEDM	Sonic	REEDM
$\overline{fb}$, unstable	0.06±0.04	0.12±0.04	0.16±0.03	-0.10±0.04
$\overline{fb}$, stable	0.07±0.09	0.39±0.07	-0.07±0.12	0.19±0.08
$\widetilde{fb}$, unstable	0.09±0.04	0.15±0.05	0.13±0.03	-0.09±0.06
$\widetilde{fb}$, stable	0.00±0.12	0.47±0.09	-0.24±0.19	0.22±0.09
Σ_{fb}, unstable	0.35	0.40	0.32	0.38
Σ_{fb}, stable	0.41	0.34	0.56	0.39
MAD_{fb}, unstable	0.28	0.32	0.30	0.37
MAD_{fb}, stable	0.33	0.41	0.58	0.35

test indicates that the 0.06 difference for $\widetilde{fb}$ in the σ_A unstable case is significant with a 95% confidence coefficient. In the stable case for σ_A, the statistics suggest that the sonic extrapolation has substantially better performance, although the sample size is small in this case.

For σ_E, the sonic and REEDM statistics in Table 8 are nearly antisymmetric. The sonic estimates tend to overestimate in unstable conditions and underestimate in stable conditions; the REEDM estimates are just the opposite. Given the inconsistent performance of both approaches for σ_E, it is difficult to claim that one approach is better than the other.

It appears that the sonic measurements produce significantly better profiles of σ_A over land compared to the REEDM algorithm, but the results for σ_E are ambiguous. Since σ_v tends to be constant with height in a convective boundary layer whereas σ_w is not, one would expect a vertical extrapolation of σ_w to be more error prone. For example, an error in the estimation of L will directly affect σ_w and σ_E through Eq. (12), but would not affect σ_v and σ_A in the same manner. This could explain why estimating turbulence aloft based on surface measurements may often work better for the horizontal fluctuations than for the vertical fluctuations.

During the Cape MVP sessions, sonic anemometers were also located near the coast. These can in principal be used to estimate the turbulence levels over the ocean and coastal waterways. It has already been demonstrated in Section 5.1. that the REEDM algorithm consistently overestimates the turbulence in these areas except under stable conditions.

To test the utility of turbulence measurements near the coast, turbulence profiles were extrapolated vertically using Sonic C in Fig. 8, which was located on Tower 110 during

Table 9: Test statistics comparing the extrapolation of Sonic C with the REEDM algorithm for $z/h < 1$. The statistics are based on Long-EZ turbulence observations collected over the sea.

	σ_A		σ_E	
Stat	Sonic	REEDM	Sonic	REEDM
n	89	89	89	89
$\overline{fb}$	0.33±0.06	0.67±0.07	0.23±0.08	0.48±0.08
$\widetilde{fb}$	0.26±0.10	0.75±0.13	0.26±0.16	0.57±0.11
Σ_{fb}	0.59	0.67	0.77	0.74
MAD_{fb}	0.65	0.76	0.95	0.83

Table 10: Test statistics for extrapolation of Sonic C data for onshore and offshore cases. The statistics are based on Long-EZ measurements collected over the sea.

	σ_A		σ_E	
Stat	Onshore	Offshore	Onshore	Offshore
n	23	66	23	66
$\overline{fb}$	0.24±0.11	0.36±0.07	0.13±0.16	0.26±0.10
$\widetilde{fb}$	0.12±0.19	0.28±0.11	0.09±0.17	0.36±0.22
Σ_{fb}	0.52	0.61	0.77	0.77
MAD_{fb}	0.53	0.69	0.78	0.96

Sessions 2 and 3. The anemometer was placed on the tower at 50 m AGL. The vertical extrapolation to the Long-EZ flight altitudes was done using the procedure described at the top of this section.

Table 9 shows the test statistics comparing both the Sonic C extrapolations and the REEDM algorithm with Long-EZ measurements over the sea. The sonic estimates show a significant reduction in overall bias—about half of that observed with the REEDM algorithm. They are still too large compared to the Long-EZ measurements, however. One explanation for this is that the Tower 110 measurements should be more representative of sea conditions for onshore winds. The data were therefore separated into onshore cases with wind directions between 30° and 150°, and offshore cases for other directions. The statistics for the onshore and offshore cases are given in Table 10.

Onshore winds do seem to produce lower biases. Differences between the onshore and offshore cases can be tested for significance using a standard t test (Sachs 1984, section 3.6.2) and the nonparametric U test (Sachs 1984, section 3.9.4). Both tests indicate that the onshore-offshore differences are not significant with a 95% confidence coefficient. This lack is significance is partly due to the relatively small number of samples that are available.

Table 11: Same as Table 9, but for the Indian River data.

	σ_A		σ_E	
Stat	Sonic	REEDM	Sonic	REEDM
n	94	94	94	94
$\overline{fb}$	-0.06±0.04	0.41±0.05	-0.05±0.04	0.27±0.05
$\widetilde{fb}$	0.00±0.043	0.52±0.04	-0.01±0.08	0.35±0.05
Σ_{fb}	0.40	0.48	0.44	0.47
MAD_{fb}	0.38	0.43	0.40	0.42

Table 12: Same as Table 10, but for the Indian River data.

	σ_A		σ_E	
Stat	Onshore	Offshore	Onshore	Offshore
n	19	75	19	75
$\overline{fb}$	0.13±0.069	-0.11±0.047	0.018±0.086	-0.073±0.055
$\widetilde{fb}$	0.15±0.07	-0.065±0.06	0.16±0.14	-0.054±0.09
Σ_{fb}	0.31	0.41	0.37	0.45
MAD_{fb}	0.27	0.40	0.29	0.43

The Sonic C data can also be tested with the Indian River data set. The statistics for this case are given in Table 11. In this case, the use of the sonic data has eliminated much of the bias seen in the REEDM estimates. In Table 12, the Indian River statistics are separated into onshore and offshore cases, based on the same criteria discussed previously. These results are rather ambiguous, although there is some evidence of overestimation for the onshore cases and underestimation for the offshore cases. Only the onshore-offshore differences for σ_A are statistically significant.

7. Conclusions

The turbulence data collected by the Long-EZ aircraft at Cape Canaveral has been used in this report to evaluate the climatological turbulence algorithm that comes with the REEDM dispersion model. This algorithm is still used for operations during rocket launches at the Cape. Based on the statistical comparisons of the algorithm and an evaluation of the spatial variability of the turbulence at the Cape, the following results were obtained.

- The boundary-layer structure and turbulence levels at Cape Canaveral can show large spatial variations. The depth of the boundary layer over the sea can be far different than over the land, and daytime turbulence levels over the sea can be smaller by a factor of two or more than those over the land. At night, the situation can be reversed, with higher turbulence levels over the sea.

- Above the boundary layer, the REEDM algorithm uses a default value of 1° for both σ_A and σ_E. The measured values for the Long-EZ were about 50% larger—closer to 1.5°. One caveat with this result is that any noise present in the Long-EZ system will have proportionally greater influence when the turbulence is light. Hence, it is possible that system noise has somewhat inflated the Long-EZ measurements.

- Superficially, the REEDM algorithm appears to perform fairly well over the inland portions of the Florida Peninsula. Further inspection reveals, however, that this result is partly due to a cancellation of errors rather than consistent performance. For σ_A, the algorithm tended to overestimate by about 30% in stability class C (slightly unstable). This was partially canceled by underestimation for B (moderately unstable) and E (stable) stability classes. For σ_E, the model showed large underestimates for classes B and D (near-neutral), which were partially offset by small overestimates for the other stability classes.

- Over the ocean and the Indian River near Titusville, the REEDM algorithm consistently overestimated the turbulence in all stabilities but class E. This overestimation was in the range of 60–200% for σ_A and 30–125% for σ_E.

- The limited amount of data for stable conditions (class E) makes it difficult to draw conclusions. However, there is a tendency for the REEDM algorithm to underestimate the turbulence over water under these conditions. This is expected given that the algorithm is designed for use over land.

- The REEDM algorithm's turbulence estimates were slightly higher when using a rawinsonde wind profiles rather than a combination of data from the Long-EZ aircraft and the XMR tower. This was due partly to slightly lower near-surface wind speeds and partly to the rawinsonde winds often showing a wind-speed maximum near 100 m AGL. The overall influence of using the rawinsonde winds was fairly small, however.

- Over the inland portion of the Florida Peninsula, significantly better estimates of σ_A were obtained by extrapolating sonic anemometer measurements upward rather than using the REEDM algorithm. The use of sonic measurements did not significantly improve the σ_E estimates. One explanation for this is that σ_w has a more complicated variation with height in the boundary layer than σ_v, and thus it is more sensitive to errors in the vertical extrapolation.

- When the turbulence over the sea near the Cape was estimated using a sonic anemometer near the coast, the bias in the estimates was only about half of that obtained using the REEDM algorithm. When only onshore winds were considered, the bias in the sonic estimates was reduced even further. However, the differences between the onshore and offshore cases was not statistically significant at a 95% confidence level, mainly because the sample size was rather small.

- The sonic near the coast was significantly better than the REEDM algorithm at estimating the turbulence over the Indian River near Titusville. In fact, the overall bias was near zero for these sonic estimates. Comparison of onshore and offshore

cases suggest that the sonic extrapolations overestimate slightly for onshore winds and underestimate slightly for offshore winds, but these differences were not statistically significant.

Overall, these findings suggest that the REEDM algorithm performs rather poorly at the Cape, particularly over water bodies. The sonic anemometer estimates almost always were superior in estimating σ_A and were also superior in estimating σ_E over the water. This supports the contention that on-site turbulence measurements are superior to stability-class algorithms at Cape Canaveral and also supports the recommendation made by Eckman et al. (1996) that turbulence instrumentation be installed at the Cape.

The on-site tests performed in this report were based solely on near-surface sonic anemometer measurements. Assumptions were therefore required to extrapolate upward through the boundary layer. These assumptions could be eliminated if profiling instruments such as sodars were installed at the Cape. Careful tests would be required, however, to ensure that such instruments provide an accurate portrayal of the turbulence field over the Cape. The data discussed in this report demonstrate that the turbulence near the Cape shows significant spatial variability, so the proper placement of turbulence instruments is crucial. Another issue to be considered is that the data sampling rate and averaging time limit the range of eddy scales that can be resolved with an instrument. When turbulence measurements from this instrument are used in a dispersion model, care must be taken to ensure that the resolved range of scales is consistent with the model's assumptions.

Although the sonic estimates performed better than the REEDM algorithm in estimating turbulence over the ocean, they still systematically overestimated σ_A and σ_E during neutral and unstable conditions. This overestimation was somewhat smaller for onshore flows, but it was still present. Better estimates over the ocean could of course be obtained by placing a turbulence instrument on a platform off the coast, but this is likely to be prohibitively expensive. One possible alternative, which could be considered as a future extension to the work discussed here, is to attempt to develop an algorithm for estimating turbulence levels over the sea based on measurements near the shoreline.

The evaluations in this report have also pointed out some of the shortcomings of the REEDM model itself. The model assumes that a single vertical turbulence profile is valid for the entire model domain and as a corollary that the boundary-layer depth does not vary with location. Both assumptions are frequently invalid at the Cape. Spatial variations in the wind speed and direction were not investigated in this report, but they will also cause errors in the REEDM dispersion estimates.

The spatial turbulence variations at the Cape were not limited to a narrow region at the coast. For example, the turbulence levels observed over the Indian River near Titusville were typically in between those observed over the ocean and those observed inland towards Orlando. Much of REEDM's total domain is therefore part of a boundary-layer transitional region between oceanic conditions and conditions over inland Florida.

8. Acknowledgements

This work was performed as part of an inter-agency agreement between the NOAA Atmospheric Turbulence and Diffusion Division (ATDD) and the U. S. Air Force. The sonic anemometer data used in the report were collected by a team led by Dr. Tilden Meyers of ATDD.

References

Atkins, N. T. and R. M. Wakimoto, 1997: Influence of the synoptic-scale flow on sea breezes observed during CaPE. *Mon. Wea. Rev.*, **125**, 2112–2130.

Atkins, N. T., R. M. Wakimoto, and T. M. Weckwerth, 1995: Observations of the sea-breeze front during CaPE. part II: Dual-Doppler and aircraft analysis. *Mon. Wea. Rev.*, **123**, 944–969.

Auble, D. L. and T. P. Meyers, 1992: An open path, fast response infrared absorption gas analyzer for H_2O and CO_2. *Bound.-Layer Meteor.*, **59**, 243–256.

Bjorklund, J. R., 1990: User's manual for the REEDM Version 7 (Rocket Exhaust Effluent Diffusion Model) computer program. Technical Report TR-90-157-01, H. E. Cramer Company, Inc., prepared for Eastern Space and Missile Center, Patrick Air Force Base, FL, 279 pp.

Brown, E. N., C. A. Friehe, and D. H. Lenschow, 1983: The use of pressure fluctuations on the nose of an aircraft for measuring air motion. *J. Climate Appl. Meteor.*, **22**, 171–180.

Byers, H. R. and H. R. Rodebush, 1948: Causes of thunderstorms of the Florida Peninsula. *J. Meteor.*, **5**, 275–280.

Caughey, S. J. and S. G. Palmer, 1979: Some aspects of turbulence structure through the depth of the convective boundary layer. *Quart. J. Roy. Meteor. Soc.*, **105**, 811–827.

Cramer, H. E., F. A. Record, and J. E. Tillman, 1966: Round Hill turbulence measurements, vols. II, III IV, and V. Technical Report Tech. Report ECOM-65-G10, Atmospheric Sciences Laboratory, Fort Huachuca, Arizona.

Crawford, T. L. and R. J. Dobosy, 1992: A sensitive fast-response probe to measure turbulence and heat flux from any airplane. *Bound.-Layer Meteor.*, **59**, 257–278.

Eckman, R. M., 1994a: Influence of the sampling time on the kinematics of turbulent diffusion from a continuous source. *J. Fluid Mech.*, **270**, 349–375.

—, 1994b: Re-examination of empirically derived formulas for horizontal diffusion from surface sources. *Atmos. Environ.*, **28**, 265–272.

Eckman, R. M., C. J. Nappo, and K. S. Rao, 1996: Rocket Exhaust Effluent Diffusion Model (REEDM) verification and sensitivity study. NOAA Technical Memorandum ERL ARL-214, NOAA Air Resources Laboratory, Silver Spring, Maryland, 56 pp.

Eckman, R. M., T. L. Crawford, E. J. Dumas, and K. R. Birdwell, 1999: Airborne meteorological measurements collected during the Model Validation Program (MVP) field experiments at Cape Canaveral, Florida. NOAA Technical Memorandum ARL/ATDD-233, NOAA Air Resources Laboratory, Silver Spring, Maryland, 54 pp.

Efron, B. and R. J. Tibshirani, 1993: *An Introduction to the Bootstrap*. Chapman & Hall, New York.

Hanna, S. R., 1989: Confidence limits for air quality model evaluations, as estimated by bootstrap and jackknife resampling methods. *Atmos. Environ.*, **23**, 1385–1398.

Hanna, S. R., G. A. Briggs, J. Deardorff, B. A. Egan, F. A. Gifford, and F. Pasquill, 1977: AMS workshop on stability classification schemes and sigma curves—summary of recommendations. *Bull. Amer. Meteor. Soc.*, **58**, 1305–1309.

Hanna, S. R., G. A. Briggs, and R. P. Hosker, Jr., 1982: *Handbook on Atmospheric Diffusion*. U. S. Department of Energy, Technical Information Center, dOE/TIC-11223.

Hicks, B. B., 1985: Behavior of turbulence statistics in the convective boundary layer. *J. Climate Appl. Meteor.*, **24**, 607–614.

Holtslag, A. A. M. and F. T. M. Nieuwstadt, 1986: Scaling the atmospheric boundary layer. *Bound.-Layer Meteor.*, **36**, 201–209.

Irwin, J. and M. Smith, 1984: Potentially useful additions to the Rural Model Performance Evaluation. *Bull. Amer. Meteor. Soc.*, **65**, 559–568.

Irwin, J. S., 1983: Estimating plume dispersion—a comparison of several sigma schemes. *J. Climate Appl. Meteor.*, **22**, 92–114.

Kamada, R. F., G. E. Start, R. P. Hosker, Jr., J. T. Knudtson, and H. L. Lundblad, 1997: MVP: Elevated SF_6 puff/plume releases from 1–1200 m at Cape Canaveral, FL. In *Proceedings of the Sixth Topical Meeting on Emergency Preparedness and Response, Vol. 1*, American Nuclear Society, 43–46.

Kruskal, W. H. and W. A. Wallis, 1952: Use of ranks in one-criterion variance analysis. *J. Amer. Statist. Assoc.*, **47**, 583–621.

Lenschow, D. H., X. S. Li, C. J. Zhu, and B. B. Stankov, 1988: The stably stratified boundary layer over the Great Plains. *Bound.-Layer Meteor.*, **42**, 95–121.

Lumley, J. L. and H. A. Panofsky, 1964: *The Structure of Atmospheric Turbulence*. Wiley-Interscience, New York.

Moeng, C.-H. and P. P. Sullivan, 1994: A comparison of shear- and buoyancy-driven planetary boundary layer flows. *J. Atmos. Sci.*, **51**, 999–1022.

Neumann, C. J., 1971: The thunderstorm forecasting system at the Kennedy Space Center. *J. Appl. Meteor.*, **10**, 921–936.

Panofsky, H. A. and J. A. Dutton, 1984: *Atmospheric Turbulence, Models and Methods for Engineering Applications*. John Wiley & Sons, New York.

Panofsky, H. A., H. Tennekes, D. H. Lenschow, and J. C. Wyngaard, 1977: The characteristics of turbulent velocity components in the surface layer under convective conditions. *Bound.-Layer Meteor.*, **11**, 355–361.

Pasquill, F., 1961: The estimation of the dispersion of windborne material. *Meteor. Mag.*, **90**, 33–49.

Reed, J. W., 1979: Cape Canaveral sea breezes. *J. Appl. Meteor.*, **18**, 231–235.

Sachs, L., 1984: *Applied Statistics, A Handbook of Techniques*. Springer-Verlag, New York, second edition.

Start, G. E. and D. Hoover, 1995: Model validation program, Cape Canaveral, Florida, draft report, NOAA Air Resources Laboratory, Field Research Division, Idaho Falls, ID.

Swanson, R. N. and H. E. Cramer, 1965: A study of lateral and longitudinal intensities of turbulence. *J. Appl. Meteor.*, **4**, 409–417.

Tangirala, R. S., K. S. Rao, and R. P. Hosker, Jr., 1992: A puff model simulation of tracer concentrations in the nocturnal drainage flow in a deep valley. *Atmos. Environ.*, **26A**, 299–309.

Turner, D. B., 1964: A diffusion model for an urban area. *J. Appl. Meteor.*, **3**, 83–91.

USAFETAC, 1986: Climatic database users handbook no. 4, DATSAV2 surface. Report USAFETAC/UH-86/004, U. S. Air Force Environmental Technical Applications Center, Asheville, NC.

Walpole, R. E. and R. H. Meyers, 1978: *Probability and Statistics for Engineers and Scientists*. Macmillan Publishing Co., New York, second edition.